Chapter 2

Seismic Modeling

This chapter presents information about seismic modeling. Topics range from why we perform modeling in the first place through a brief overview of the mathematics involved in several different types of modeling.

Primary Concerns

One primary concern in seismic imaging necessarily focuses on determination of the true subsurface medium. Clearly, the accuracy of this information significantly impacts all aspects of the exploration process. Even when we do not have a completely detailed visualization of what is below us, a reasonable concept can provide guidelines for surface acquisition that improves subsurface imaging. The underlying Earth model strongly influences what we must do to migrate the data successfully and produce an optimum image.

Another primary concern focuses on which of the myriad available imaging algorithms has the best chance of producing the highest quality image. Making this choice requires an understanding of the most important such technology. Because algorithm development and implementation is a highly mathematical endeavor, acquiring this understanding can be quite difficult.

A third concern arises from the fact that, in general, the Earth does not respond well to high frequency sources since high frequency sound waves are absorbed rather quickly. Depending on rock type they penetrate only to a few thousand meters. On the other hand, low frequency sound waves are known to provide narrow bandwidth images at depths in excess of 30 or 40 kilometers.

Electromagnetic waves are frequently characterized by their penetration depth or their so called skin temperature. Although claims to the contrary abound, the skin

temperature of most electromagnetic waves is only on the order of a few hundred meters. This means that to the extent possible, changes in magnetic parameters can be observed only from approximately half of this depth. This is far too shallow to be of much use in exploration. This lack of ability to penetrate deeply into the Earth's interior eliminates most high frequency sources, and strongly implies that we cannot use light, electromagnetic, or radar sources to measure and image the Earth at the depths of interest.

Because of these issues, our best option is to use relatively low frequency sound sources on the order of a few hundred Hertz. When higher frequency sources are routinely available, their responses will be easily incorporated into the general imaging workflow, but until that happens, we must focus on low frequency data sets to achieve our exploration goals. We now know that, from an inversion point of view, accurately determining the subsurface velocity is easier when the low frequency portion of the frequency band is full. High frequencies are certainly important but have much less impact on the velocity estimation problem then lower frequencies. While somewhat contrary to intuition, the importance of very low frequency data cannot be denied.

Perhaps the final concern in seismic imaging is having a clear understanding of how sound propagates. Given a decent understand of the types of rocks we may encounter, this concern can be resolved directly through seismic synthesis or modeling. The ability to generate realistic responses to practical and physical seismic sources should move us a long way down the path toward near optimal application of the entire imaging process

Given these simple concerns, this section attempts to use mathematically based formulations for digitally synthesizing seismic data in the hopes that the issues raised above can be clarified in a relatively simple and intuitive manner.

Three Earth Models

Earth models, as we understand them, have the following three basic formulations:

- purely isotropic or acoustic
- isotropic elastic
- anisotropic

Acoustic or Fluid

Earth models, as we understand them, have three basic formulations. The first is what we usually call purely isotropic or acoustic. Acoustic models are based on the assumption that the only physical parameters defining wave propagation are density, $\rho(x,y,z)$, and interval or instantaneous velocity $v(x,y,z)$. Only fluids can be described by these two properties, but because propagation in such environments can be simulated efficiently, they are the most prevalent at this writing. Empirical evidence also seems to suggest that in many geologic settings the real Earth does not vary much from this assumption.

Isotropic Elastic

Isotropic elastic models are described by density, compressional velocity, and shear velocity. The notation for these parameters is $\rho(x,y,z)$, $v_p(x,y,z)$, and $v_s(x,y,z)$. Isotropic elastic models support two wavefields, one of which is a compressional wave and the other is a shear wave. Compressional waves in such models are identical to those in acoustic models. They are characterized by particle motions consistent with what might be called compression and rarefaction where the particle vibrations are normal to the direction of propagation. In contrast, we tend to think of waves where the the particle motion is tangential to the direction of propagation as shear waves. As a point of fact, the truth is probably somewhat different. Simulations tend to support the conclusion that the compressional wave is what we would record if we were to measure purely vertical particle motion and the shear wave is the one characterized by purely horizontal particle motions. The speed of shear waves is frequently much slower then the velocity of the compressional wave. Nevertheless, shear and compressional waves continually interact and convert from one to the other as the propagation progresses. Thus, if we are to successfully handle isotropic elastic data, we must acquire something at least directly related to the vertical and horizontal particle motions. In other words, we have to acquire *vector* data.

Anisotropic

Anisotropic models represent the Earth at its most complex. For our purposes, a model is said to be anisotropic whenever the sound speed is a function of the angle of propagation. In models of this type, not only does the velocity of sound vary with propagation angle, but there are three possible propagating modes at any given instant. One is our familiar compressional wave and the other two are shear waves, each of which propagates with its own local angle-dependent velocity profile.

Over the last 20 or so years we have come to specify what we might call the first realistic anisotropic models by density $\rho(x,y,z)$, vertical velocity $v_p(x,y,z)$, shear horizontal velocity $v_s(x,y,z)$ and three additional parameters, $\delta(z,y,z)$, $\varepsilon(x,y,z)$, and $\gamma(x,y,z)$. Models described by these "Thomsen" parameters are the so called vertically transverse isotropic or VTI models. Anisotropic VTI models have a very convenient form of symmetry that makes using them somewhat easier and less computationally complex then more complex versions of anisotropy. It is reasonable to expect anisotropic models to become the norm in future exploration exercises. In this case true anisotropic processing will also require the acquisition of vector data. The difference between this and isotropic elastic acquisition is that each vector has three components.

Summary

Regardless of the source we use, the Earth's response always contains compressional and at least one, but most probably, two shear wavefields. Thus, the expected Earth model is quite complex. While we may not have the ability to estimate the necessary parameters to image the recorded multicomponent data, there are many algorithms for doing so. It makes sense to at least understand the kinds of data we might expect to record and what it might look like. The basic idea of using modeling to help us understand the recordings has a significant history in the exploration for hydrocarbons. As this book progresses, we will attempt to define the various models currently in vogue and make some additional comments about how the required parameters might be estimated from our acoustical recordings.

Seismic Acquisition: The Basic Idea

The basic idea underlying seismic acquisition is shown in Figure 2-1. The application of a sound source at a fixed point on the surface of the Earth produces a down-going wavefield. As the wavefield propagates, it is, hopefully, reflected as an up-going wavefield that is recorded on a series of receivers located near the surface. The job of modeling is to simulate this thought experiment as accurately as possible. From a physical point of view the model is viewed as a collection of *particles* that move (compress and expand or shear) under the influence of the sound source. As we can easily infer from Figure 2-1 such compression and rarefaction can be quite complex and occur in any direction at any given time instant.

As we progress through this book, we will see that there are many approaches to synthesizing seismic data in both simple and complex Earth models. Each approach is based on a unique approximation to a governing wave equation. Each approximation has its own unique set of limitations that compromises the accuracy of the final synthetic. In the past, these approximations were a necessary evil fostered by the computational limits of the era. The list of questions posed in Figure 2-1 hint at some of the limitations of the various approximations. Ranging from algorithms based on rays (infinitely narrow paths), to wavefields that travel in only one direction, and then to wavefields traveling in all directions, these limitations can have a serious impact on the quality of both the modeling and the migration algorithm under consideration. As computers become more and more efficient, these compromises will fall by the wayside and be fully replaced by the most accurate method available for the given data.

Figure 2-1. The basic seismic acquisition concept.

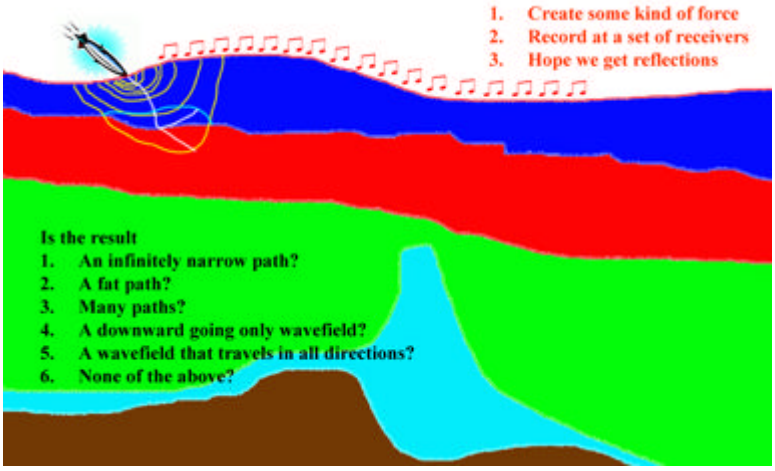

Why Model?

Modeling is fundamental to imaging, and I hope to convince you that modeling and migration are identical; that is, if you know how to do one, you know how to do the other. Consequently, it is extremely important that you understand how to synthesize seismic responses that are as close as possible to what we physically measure in the real world.

Determining Reflector Location

Before computers, simple straight-ray methods were used to determine the important parameters involved in figuring out the true sub-surface location of recorded reflected events. Figure 2-2 demonstrates the process.

Figure 2-2. Raytracing in a $v(z)$ medium.

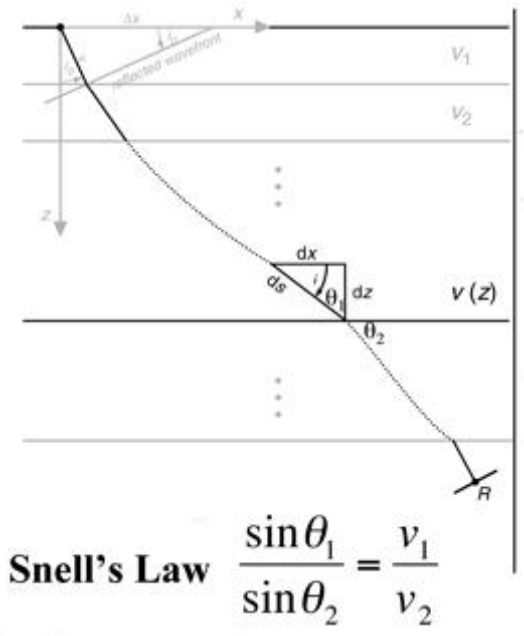

Computing the ray direction from one layer to the next requires adherence to Snell's law, Equation 2-1 or Equation 2-2. See the section on Curved Rays in Chapter 3 for information about Snell's law.

(2-1)
$$\frac{\sin\theta_1}{\sin\theta_2} = \frac{v_1}{v_2}$$

(2-2)
$$\frac{\sin\theta_1}{v_1} = \frac{\sin\theta_2}{v_2}$$

Thus, the only required elements for this form of modeling are the ability to compute the sine of angles, a ruler, and perhaps a protractor. What is important is that for a given source on the surface the normal incident ray that travels from the source to a reflector and back to the source-receiver location is uniquely determined by either the dip of the reflector or by the takeoff angle at the surface.

As we will see, this particularly simple concept is fundamental to both migration and modeling. We can estimate what we call apparent dips from seismic sections, and then compute the true dip of the reflector, along with a given velocity. Simultaneously, we can compute the surface distance from the given shot point to the surface projection of the subsurface reflector location, thereby constructing a "migrated" image.

Geologic Complexity

Perhaps the earliest and one of the most compelling reasons for modeling was presented by Frank Rieber's in his 1936 Geophysics paper. Quoting Rieber:

> The usual form of reflection seismograph operates satisfactorily over simple structural conditions, but frequently fails to obtain part or all of the desired information when structures are steeply folded, faulted or otherwise complicated. The reasons for this are plainly evident if the paths of the waves in the earth can be visualized.

In other words, he is saying that when the geology is simple, the reflection seismogram is easy to unravel, but when the geology is complex, it is difficult. He is also saying that if we can model complex structures, we may be able to better understand the problem and then develop technologies to resolve it. From my perspective, the most amazing thing is that he proceeds to do exactly that:

> This has been done by the use of a technique originally developed for acoustical measurements.
>
> A new type of equipment and technique are briefly described, with which exploration may be carried into the more complex structural regions successfully.
>
> A miniature explosion radiates waves into various models of structure, where reflection and diffraction take place in the same manner as in the earth. The various moving waves are actually photographed in flight. A series of plates is presented, showing wave patterns in various types of structures, ranging from simple to complex.
>
> Briefly, the technique is one of shadow photography, no lens of any sort being employed. A bright electric spark, lasting only about one millionth of a second, is spaced about four feet from a photographic plate. The model of

> the structure to be investigated is placed part way between the spark and the plate, in such a position that its shadow will be photographed.
>
> If no sound waves are present in the field between the light source and the plate, the shadow of this model will be the only thing shown in the photograph. The rest of the field will be uniformly exposed to the light from the spark and will correspondingly show uniform photographic density.
>
> If an abrupt sound wave happens to be passing through the field, however, the light from the spark will be bent slightly at the places where it passes through the denser air of the wave front. This bent light will be superposed upon other illumination arriving directly on the plate from the spark, thereby causing a dark line. The part of the plate from which the bent light was diverged will show, correspondingly, as a lighter line.

Thus, Rieber explains why he thinks modeling is important, and then proposes a solution to both the modeling and the visualization problem. The *why* in Rieber's case was to figure out how to interpret seismic shot records that were considered uninterpretable at the time. In the 1930's, tedious hand calculations were the only available methods for placing an event on a shot record at its correct (or nearly correct) subsurface position. These early migration methods were not well suited to positioning anything but simple reflected events. While the response of a syncline was not difficult to unravel, what Rieber's paper showed was that the so-called "no record zones" were in reality areas with even moderately complex geology. Salt structures of the size and shape we see today were generally figments of the imagination.

Figure 2-3 demonstrates the validity of Rieber's shadow method. Figure 2-3(a) shows that the response of a truncation in an otherwise constant velocity medium is a diffraction. This is a circular event that could have easily confused the typical inexperienced interpreter of the day. Part (b) shows the downward traveling wave on the edges along with the reflected wave in the center for a faulted structure. Note the clear diffractions on the left-hand side of this graphic. It is one of several similar Rieber graphics that clearly demonstrate the success of his technique. The left half of this figure shows a snapshot of the response from a syncline at some time after the explosion at the center of the image. The right half is a snapshot at a later time. What we see, particularly on the top half of the figure, is the characteristic bow-tie reflection from the syncline.

Figure 2-3. Rieber's shadow graphs of the response of simple geologic structures.

(a). Reiber's snapshots of the response of truncated structures.

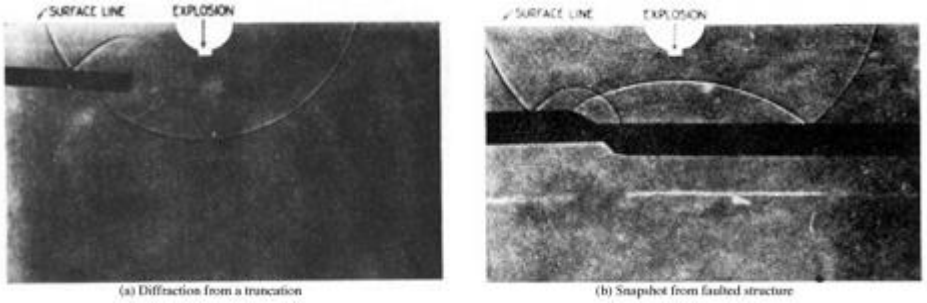

(a) Diffraction from a truncation (b) Snapshot from faulted structure

(b). Reiber's snapshots of the response of a syncline

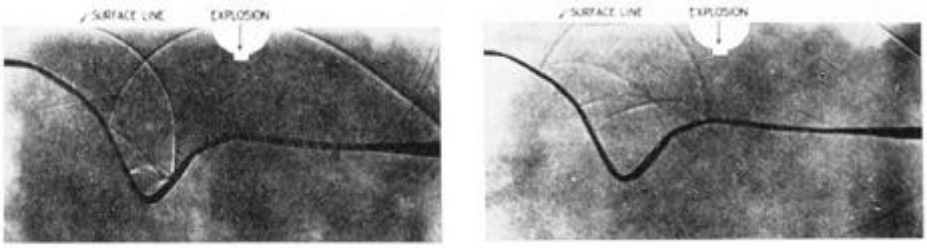

At the time of Rieber's research, the complexity of the seismic response was not well understood, and, consequently, detecting or even recognizing dip on these records was problematic. Figure 2-4 shows that Rieber understood this as well, and formulated a method for more or less automatic detection of the associated dips. It represents what is believed to be one of the first ever utilization's of what is now called slant stacking. Note that it is applied to a shot record and really detects the angle at which the given reflection emerges. The dip detector first estimates the emergence angle of a reflected wavefield at the receiver locations, which can be computed from $\frac{\Delta t}{\Delta x} = \frac{\sin\theta}{v}$. Given the emergence angle and the velocity of the wavefield (which was assumed constant in Rieber's day), we can directly calculate the location and dip of the reflector from which the wavefield came. As we will see in later chapters, this emergence angle data and the directly related subsurface dip are crucial in all modern migration methodologies.

Figure 2-4. Rieber's approach to detecting dip.

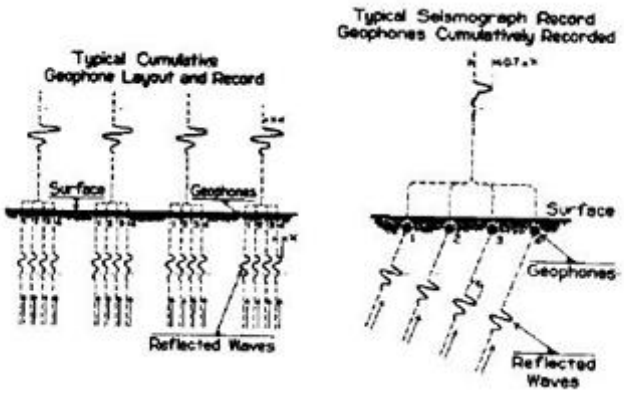

Hypothesis Testing

A more modern reason behind data synthesis is what can be called hypothesis testing. An example of this is displayed in Figure 2-5. The left hand side of this figure is an arbitrary line slice taken through a 3D prestack depth migration of a seismic data set from the Gulf of Mexico survey. It was chosen to be as close as possible to a true dip line. The right graphic is an image constructed from 2D isotropic elastic data synthesized over a 2D structure constructed from the 3D migration velocity field along with top and base salt interpretations.

Figure 2-5. Modeling multiples.

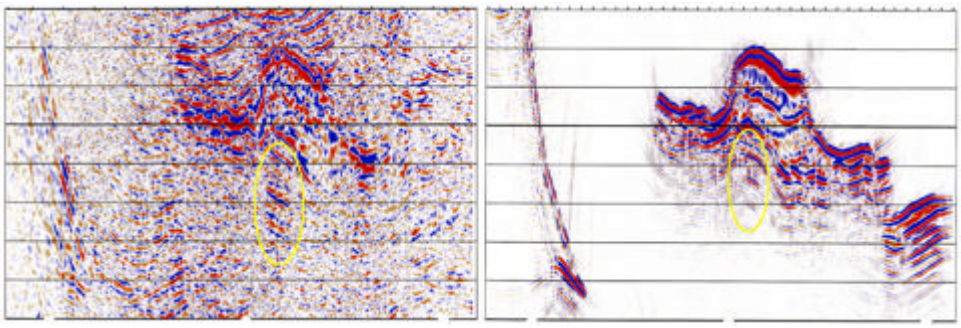

When mapped in 3D, the circled amplitude package appears to define a stacked set of hydrocarbon bearing reservoirs with significant potential. Thus, the hypothesis in this case is that the package is a valid prospect. To test this hypothesis, a 2D acoustic Earth model was constructed. The model velocity was taken to be the migration velocity with a top and base of salt used to define the salt body. Although not shown, the model includes shear velocities below the water layer, and, consequently, some converted waves have been imaged on the section.

The right side of Figure 2-5 shows the result of the modeling under the assumption that the surface of the water is not reflective. Thus, any repetitive events cannot be from water column multiples. The clear evidence of multiple amplitudes in a setting where such amplitudes cannot be due to the water layer, confirms the hypothesis that the amplitudes are from peg-leg multiples or converted ray events.

There are, of course, many other ways to utilize modeling to answer various hypotheses that are not directly related to verifying that some event or anomaly is noise. We can also build models to compare various alternative model parameters in an attempt to quantify observed amplitude versus offset or amplitude responses. In a subsequent section on full waveform inversion, we will demonstrate the importance of low frequency acquisition in the specification of the earth velocity field.

Acquisition

An important recent utilization of modeling by Carl Regone at BP dealt directly with trying to verify that wide azimuth acquisition is superior to narrow acquisition. What these studies showed was that, as actually assumed by the mathematics, wide azimuth acquisition produces superior results in all settings. We will investigate this issue in the chapter on Data Acquisition.

Waves and Wavefields

As described in Figure 2-6, wavefields are characterized and described by several well known terms:

- f = Frequency = cycles/second
- ω = Angular Frequency = radians/second = $2\pi f$
- $\frac{v}{f}$ = Wavelength = meters/cycle
- $k = \frac{\omega}{v}$ = Temporal Wave Number
- k_x = Spatial x (XLINE) Wave Number
- k_y = Spatial y (LINE) Wave Number

Figure 2-6. A single frequency sinusoid (wavefield) with amplitude $A(x, y, z, \omega)$

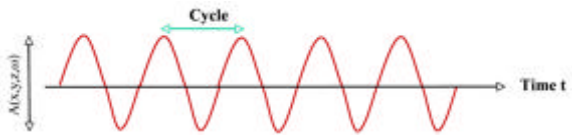

These terms completely characterize wavefields in space-time, frequency-space, and frequency-wavenumber. We can think of wavefields as actually being the sums of sinusoidal style waves having the general form of Equation 2-3, where $A = A(x, y, z, \omega = 2\pi f)$ is a positive amplitude as a function of spatial position (x, y, z) and frequency, and $\varphi = \varphi(x, y, z, t)$ is the so-called wavelet phase.

(2-3) $$U(x, y, z, t) = \sum_{\omega} A\left[\cos(\omega t + \varphi) + \imath \sin(\omega t + \varphi)\right]$$

The main point is that the wavefields actually exist in three-dimensional space-time and can be characterized in many different ways. While we cannot record the full three dimensional response of any given source, the wavefield due to such a source is in fact four dimensional and effectively exists at each point where energy from the source exists. In this book, we will mostly be concerned with wavefields measured on one surface, typically where $z = 0$. But, as is the case for VSPs, we also record seismic wavefields at locations with $z > 0$.

Figure 2-7 further clarifies what we mean by Equation 2-3. As any given sinusoid propagates through the Earth, its wavelength and amplitude change as functions of both reflection strength and sound speed. Although not shown in the figure, these quantities can also change purely as a function of the material through which they are propagating.

Figure 2-7. Wavefield in space at two different velocities. Note that the wavelength and the amplitude can change purely as a function of velocity.

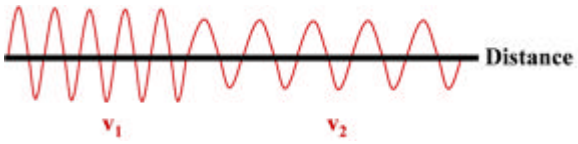

The Scalar Wave Equations

From the author's perspective, current state-of-the art practice in digital synthesis of seismic wavefields is usually based on one of four wave equation styles.

- The simplest style is called the *scalar* wave equation governing particle motion. Traditionally, this equation involves only compressional style waves and provides a wavefield describing particle motion; density is assumed constant.
- The first and second order formulations of what is usually referred to as the *stress-strain* equations can synthesize both compressional and shear wave data, although at considerable expense in 3-D. Thus, in this case, the equations govern what can be considered vector propagation. In the simplest case, there are two wavefields, one compressional and one shear. In the more complex case, there are three wavefields, one compressional and two shear. The stress-strain versions are clearly the most interesting because they allow for the most complex anisotropic wavefield propagation methods.
- The *pressure* formulation of the wave equation includes density in a form that can be used directly for synthesizing marine style acquisition.

The 1-D Scalar Wave Equation

In this section, we derive a simple one-dimensional version of the so-called scalar wave equation. Wavefields satisfying the various forms of the wave equation are currently our best guess as to how low-frequency-sound energy propagates through the Earth. As we will see, different media require specialized equations, but the basic synthesis or modeling principles remain remarkably similar.

We can gain insight into how particle movement (wave propagation) is governed by considering a simple one-dimensional model. We will start by thinking of the media as a series of discrete particles loosely connected by some form of restraint. Figure 2-8 shows a series of masses, m, connected together through a series of springs under tension, k. A source at one end of the chain creates a wavefield that travels up and down the chain.

Figure 2-8. A simple one-dimensional model.

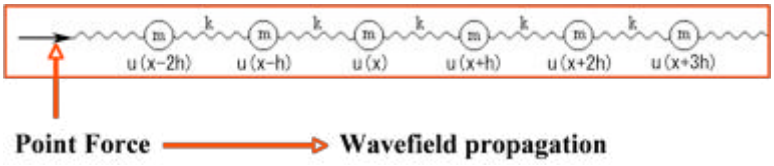

If a force is applied at one end of this one-dimensional model, the mass $u(x)$ at x reacts with and is acted on by masses $u(x - h)$ and $u(x + h)$. Each such mass accelerates and

decelerates as the wavefield generated by the source propagates up and down the model. Note that, although we have suppressed it in the notation, the fact is that $u(x) = u(x,t)$. In general, we think of each of the masses, $u(x)$, as particles that move back and forth as time progresses. What we see is a wave passing up and down the model.

Describing particle movement is accomplished through the use of two fundamental laws of physics, Newton's second law of motion, that is, *force is equal to mass times acceleration*, and Hooke's Law.

> In physics, Hooke's law of elasticity is an approximation that states that the amount by which a material body is deformed (the strain) is linearly related to the force causing the deformation (the stress). Materials for which Hooke's law is a useful approximation are known as linear-elastic or *Hookean* materials.

In mathematical form, Newton's law is given in Equation 2-4, where a is acceleration and m is the particle mass.

(2-4) $$F = ma$$

The force caused by acceleration is what you feel when you step on an automobile's accelerator. In the context of Figure 2-8, acceleration is the rate of change in velocity with respect to time. Thus, for the particle at $u(x)$, Newton's second law becomes Equation 2-5, where $\tau(x,t)$ is the force per unit area, or stress, at x.

(2-5) $$\tau(x,t) = m\left[\frac{v(x,t+\Delta t) - v(x,t)}{\Delta t}\right]$$

The fact that the velocity is the change in particle position as a function of time yields Equation 2-6, and, thus, Newton's law can be written as Equation 2-7.

(2-6) $$v(x,t) = \frac{u(x,t) - u(x,t-\Delta t)}{\Delta t}$$

(2-7) $$\tau(x,t) = m\left[\frac{u(x,t+\Delta t) - 2u(x,t) + u(x,t-\Delta t)}{\Delta t^2}\right]$$

For our purposes, Hooke's law can be rephrased as:

> A *change in force* per unit length (area or volume in higher dimensions) is equal to the bulk modulus times the increase in length divided by the original length.

Because of the way in which our small particles of mass are arranged, the force $\tau(x,t) = \frac{F(x,t)}{h}$ per unit length is really determined by the action of the particles adjacent to position x. Hooke's law can be stated mathematically as Equation 2-8 or Equation 2-9.

(2-8)
$$\begin{aligned}\tau(x,t) &= \tau(x+h,t) + \tau(x-h,t) \\ &= k\left[\frac{u(x+h,t)-u(x,t)}{h}\right] + k\left[\frac{u(x,t)-u(x-h,t)}{h}\right]\end{aligned}$$

(2-9)
$$\frac{kh^2}{m}\left[\frac{u(x+h,t)-2u(x,t)+u(x-h,t)}{h^2}\right] = \left[\frac{u(x,t+\Delta t)-2u(x,t)+u(x,t-\Delta t}{\Delta t^2}\right]$$

If we suppose that there are N masses (particles), each of density ρ, then the total length is $L = Nh$, the total mass is $M = Nm = \rho$, and the total stiffness of the array is $K = k/N$, so we get Equation 2-10.

(2-10)
$$\frac{kh^2}{m} = \frac{KL^2}{M} = \frac{KL}{\rho}$$

Thus, in the limit as h and Δt approach zero, we get Equation 2-11. The quantity KL is actually Young's modulus of the medium containing m.

(2-11)
$$\frac{KL}{\rho}\frac{\partial^2 u}{\partial x^2} = \frac{\partial^2 u}{\partial t^2}$$

It turns out that the quantity $v = \sqrt{\frac{KL}{\rho}}$ is the velocity of propagation within the medium, and so we have succeeded in deriving what is normally called the one-dimensional wave equation, Equation 2-12.

(2-12)
$$\frac{\partial^2 u}{\partial x^2} = \frac{1}{v^2}\frac{\partial^2 u}{\partial t^2}$$

It is interesting to note that if we combine Equation 2-7 and Equation 2-9, and then rearrange the result in the form shown in Equation 2-13, we obtain an equation that allows us to propagate a wavefield in the one-dimensional medium due to the source $s(x_0,t)$ at position x_0.

(2-13)
$$\begin{aligned}u(x,t+\Delta t) &= 2u(x+h,t) - u(x,t-\Delta t) \\ &\quad + v^2[(u(x+h,t) - 2u(x,t) + u(x-h,t)] + s(x_0,t)\end{aligned}$$

If we begin the discussion with both mass, m, and strain, k, as functions of position, x, the velocity, $v = v(x)$, of our one-dimensional wave equation will vary as a function of position.

It is clear from Equation 2-13 that propagation at each time step is achieved through the application of appropriate weights to the wavefields at the two previous time steps. In the case where velocity varies, the weights form a *stencil* and change for each spatial position. The wavefield at time stamp $t + \Delta t$ is computed starting at the left most spatial position and continuing to the right.

Figure 2-9 demonstrates the process. Beginning at the left each spatial output point amplitude is computed as a weighted sum of spatial points from the two previous time steps, that is, $t + \Delta t$. The stencil at t is centered around the spatial output point at $t + \Delta t$ so that waves can propagate in all directions.

Figure 2-9. Graphical interpretation of a one-dimensional propagator

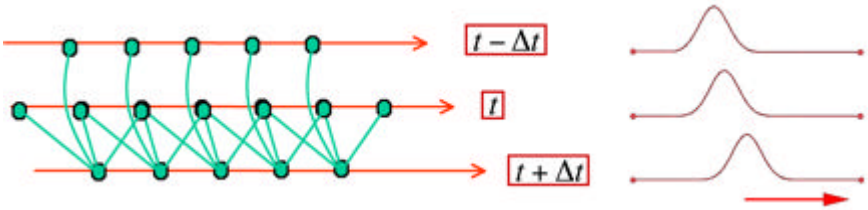

Scalar Wave Equation in Higher Dimensions

Figure 2-10 shows a simple model in two dimensions. In this case, masses, m, are connected by the equivalent of springs with tension k. A source placed as a point on the grid creates a wavefield that travels up throughout the grid in all directions.

Figure 2-10. A simple two-dimensional model.

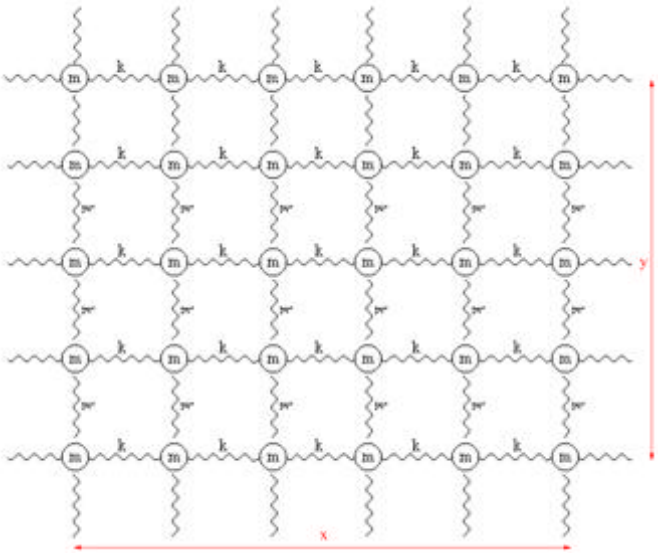

Extending the one dimensional nature of Equation 2-12 into higher dimensions is not difficult. We need only consider a two-dimensional grid of masses similar to the one-dimensional grid in Figure 2-8. Our model now has an area $A = L_x * L_y$, instead of length L, a total stiffness of $K = \frac{k}{L_x L_y}$, and total mass $M = mL_xL_y$. Our discrete equation governing wave propagation must accommodate particle motion in both the x and y directions, but, in actuality, this really only involves Equation 2-9. Thus, if we follow our approach for the one-dimensional discrete equation, Equation 2-13, we arrive at Equation 2-14.

$$\left(\frac{u(x,z,t+\Delta t) - 2u(x,z,t) + u(x,z,t-\Delta t}{\Delta t^2}\right) = \frac{kh^2}{m}\left(\frac{u(x+h,z,t) - 2u(x,z,t) + u(x-h,z,t)}{h^2} + \frac{u(x,z+h,t) - 2u(x,z,t) + u(x,z-h,t)}{h^2}\right) \tag{2-14}$$

In more compact mathematical notation, the two-dimensional Equation 2-14 becomes Equation 2-15.

$$\frac{\partial^2 u}{\partial t^2} = v^2\left(\frac{\partial^2 u}{\partial x^2} + \frac{\partial^2 u}{\partial z^2}\right) \tag{2-15}$$

After following the same procedure for a three-dimensional grid, the three-dimensional wave equation becomes Equation 2-16.

$$\frac{\partial^2 u}{\partial t^2} = v^2\left(\frac{\partial^2 u}{\partial x^2} + \frac{\partial^2 u}{\partial y^2} + \frac{\partial^2 u}{\partial z^2}\right) \tag{2-16}$$

Here, we have derived the mathematical wavefield equations for what is normally called acoustic or pure isotropic modeling. In this case, the velocity was assumed constant, but the difference between a constant velocity and variable velocity derivation is minor. Equation 2-15 and Equation 2-16 are referred to as scalar wave equations because there is only one wavefield, not a vector of two or more. Generally, the geophysical convention is to assume that z is the vertical or depth direction, but that is really just a matter of convenience. We could just as easily have used x_1 for x, x_2 for y, and x_3 for z.

Pressure Formulation of Acoustic Wave Equation

Without going into great detail, we can also derive a pressure formulation of the acoustic wave equation (see Keiiti Aki and Paul G. Richards). This equation takes the form shown in Equation 2-17.

$$\frac{\partial^2 p}{\partial t^2} = \rho(x,y,z)\, v^2(x,y,z)\left[\frac{\partial}{\partial x}\frac{1}{\rho(x,y,z)}\frac{\partial p}{\partial x} + \frac{\partial}{\partial y}\frac{1}{\rho(x,y,z)}\frac{\partial p}{\partial y} + \frac{\partial}{\partial z}\frac{1}{\rho(x,y,z)}\frac{\partial p}{\partial z}\right] \tag{2-17}$$

In contrast to the particle motion described by Equation 2-16, Equation 2-17 measures pressure changes at any given position. I like to call this the reflection formulation because of the presence of the acoustic impedance term, ρv. This equation can be put in the very compact form of Equation 2-18, where ∇ (the vector differential operator, pronounced *del*) is given by Equation 2-19.

$$\frac{\partial^2 p}{\partial t^2} = \rho v^2 \nabla \cdot \frac{1}{\rho}\nabla p \tag{2-18}$$

$$\nabla = \left(\frac{\partial}{\partial x}, \frac{\partial}{\partial y}, \frac{\partial}{\partial z}\right) \tag{2-19}$$

Ultimately, we are interested in deriving equations for more complex fully elastic wavefields, including anisotropic wavefields. These wavefields require more parameters to describe the multiplicity of wavefields that exist in such media. Before increasing the complexity of the discussion, we will focus on a graphical description of how discrete modeling works, and then turn our attention to algorithms for implementing the actual modeling exercise.

Stress-Strain Equations

As we know, isotropic elastic models are described by three familiar parameters: density, compression velocity, and shear velocity. To model elastic wavefields in such three-parameter media, we need to derive a suitable equation or set of equations that describe the wavefield propagation at any given instant. Unfortunately, these three parameters are not the most useful for this purpose. On the other hand, the required parameters are much more directly related to actual rock properties. Moreover, relating the required parameters to more useful quantities is fairly straightforward.

We begin (Equation 2-8 and Equation 2-7) by observing that Equation 2-20 is true, so that Equation 2-21 is also true.

(2-20)
$$\begin{aligned}\frac{F(x,t)}{h} &= \frac{F(x+h,t)+F(x-h,t)}{h} \\ &= k\left(\frac{u(x+h,t)-u(x,t)}{h}\right)+k\left(\frac{u(x,t)-u(x-h,t)}{h}\right) \\ &= \rho\left(\frac{u(x,t+\Delta t)-2u(x,t)+u(x,t-\Delta t)}{\Delta t^2}\right)\end{aligned}$$

(2-21)
$$\frac{\tau(x+h,t)-\tau(x,t)}{h} = \rho\left(\frac{u(x,t+\Delta t)-2u(x,t)+u(x,t-\Delta t)}{\Delta t^2}\right)$$

In continuous terms, Equation 2-21 can be restated as Equation 2-22.

(2-22)
$$\frac{\partial \tau}{\partial x} = \rho\frac{\partial^2 u}{\partial t^2}$$

Equation 2-22 is a first order partial-differential equation relating a second order change in time to a first order change in force *per unit area*. Force per unit area is generally referred to as stress, so our equation relates particle acceleration to stress. In this setting, the stress is one-dimensional and acts along or parallel to the layout of the string. There is also only one compressional wavefield described by this equation.

Stepping up to the simple isotropic elastic models described by the three familiar parameters above, means that it is necessary to include one additional wavefield in the mix, namely shear. While including just two wavefields is certainly an option, there isn't any reason not to move up to full anisotropic elasticity by incorporating two shear waves for a total of three wavefields. In three dimensions, Equation 2-22 takes the form of Equation 2-23, where $i = 1,2,3$ and we have arbitrarily chosen to set $x = x_1$, $y = x_2$, and $z = x_3$.

(2-23)
$$\frac{\partial^2 u_i}{\partial t^2} = \frac{1}{\rho}\sum_{j=1}^{3}\frac{\partial \tau_{ij}}{\partial x_j}$$

Clearly, this is a three-dimensional equation with nine stress factors, τ_{ij}, one for each of the three dimensions and wavefields. To make this into a system of equations governing the three wavefields, we must find a way to relate the stresses, τ_{ij} to the u_i. As before, Hooke's law comes to the rescue. What it says in this anisotropic case is:

> Each component of stress is linearly proportional to *every* component of strain.

Strain, which measures the deformation (compression, extension, ...) of a solid, is defined in the notation of the previous equation as Equation 2-24.

(2-24) $$E_{mn} = \frac{1}{2}\left(\frac{\partial u_m}{\partial x_n} + \frac{\partial u_n}{\partial x_m}\right)$$

The mathematical expression of Hooke's law then takes the form of Equation 2-25.

(2-25) $$\tau_{ij} = \sum_{m,n} c_{ijmn} E_{mn}$$

Inserting Equation 2-25 into Equation 2-23, we finally get the complex system ($i = 1, 2, 3$) of fully anisotropic equations of motion, Equation 2-26.

(2-26) $$\frac{\partial^2 u_i}{\partial t^2} = \sum_{m,n,j} \frac{c_{ijmn}}{\rho} \frac{\partial^2 u_m}{\partial x_n \partial x_j}$$

Symmetry

Because Equation 2-26 is three-dimensional, each of the c_{ijmn} coefficients is actually a three-dimensional volume. Even today's massive supercomputers may not have sufficient memory to handle a problem of this size.

We could easily throw up our hands at this point and give up, but, before we panic too much, we might want to analyze the situation a bit. As it turns out there are at least two things we can do to simplify the situation considerably. First, we can simplify the mathematical notation to put us into a setting where we can make some sense of the parameters, and second, we can reformulate the c_{ijmn} coefficients in a way that will make a great deal more physical sense.

We are not really interested as much in the math as we are in understanding the kinds of Earth models these c_{ijmn} coefficients define for us. We need to know how the various velocities of the wavefields that propagate in the medium are defined. We also want to see if we can understand how direction changes the speed of propagation, and then see if we can find ways to estimate parameters that can be converted into c_{ijmn} volumes so we can both synthesize data and image data we have recorded over fully elastic models.

The first simplification to the complexity of Equation 2-26 is based on the symmetry of stress and strain. Here, the ij indices representing stress can be switched so that $c_{ijmn} = c_{jimn}$. Similarly, the strain based indices can also be switched so that $c_{ijmn} = c_{ijnm}$. Finally, it is also true that $c_{ijmn} = c_{mnij}$. This triple symmetry means that the total number of c_{ijmn} volumes has been reduced to **only 21**! Thus, defining the most general model

we can imagine requires only 21 independent parameters (volumes), instead of the 81 parameters we would need without symmetry.

By applying the indexing scheme (known as the Voigt scheme) in Equation 2-27, we arrive at the 6x6 matrix shown in Equation 2-28.

(2-27)
$$\begin{array}{cccccccccc} index & ij & = & 11 & 22 & 33 & 23 & 13 & 12 \\ map & \downarrow & & \downarrow & \downarrow & \downarrow & \downarrow & \downarrow & \downarrow \\ index & k,l & = & 1 & 2 & 3 & 4 & 5 & 6 \end{array}$$

(2-28)
$$C = [c_{kl}] = \begin{bmatrix} c_{11} & c_{12} & c_{13} & c_{14} & c_{15} & c_{16} \\ c_{12} & c_{22} & c_{23} & c_{24} & c_{25} & c_{26} \\ c_{13} & c_{23} & c_{33} & c_{34} & c_{35} & c_{36} \\ c_{14} & c_{24} & c_{34} & c_{44} & c_{45} & c_{46} \\ c_{15} & c_{25} & c_{35} & c_{45} & c_{55} & c_{56} \\ c_{16} & c_{26} & c_{36} & c_{46} & c_{56} & c_{66} \end{bmatrix}$$

This matrix completely describes the unique set of 21 coefficients fully defining anisotropic elasticity. In this case, the C matrix is the most complicated form of anisotropy we can encounter. For the interested reader, this case is called “triclinic” symmetry and is probably something we will not be able to investigate computationally until computers have advance significantly beyond where they are today. Moreover, we may never be able to measure sufficient data to be able to estimate all of these parameters. Consequently, we will focus on what we consider reasonable today.

Acoustic Symmetry

In what perhaps is overkill, the C matrix takes the form shown in Equation 2-29 for a purely acoustic medium.

(2-29)
$$C = [c_{kl}] = \begin{bmatrix} \lambda & \lambda & \lambda & 0 & 0 & 0 \\ \lambda & \lambda & \lambda & 0 & 0 & 0 \\ \lambda & \lambda & \lambda & 0 & 0 & 0 \\ 0 & 0 & 0 & 0 & 0 & 0 \\ 0 & 0 & 0 & 0 & 0 & 0 \\ 0 & 0 & 0 & 0 & 0 & 0 \end{bmatrix}$$

Here, λ is the first of the two so-called “Lamè” parameters. Named after Gabriel Lamè, they are material properties (proportionality constants) that relate stress to strain. In this case, λ is directly related to the bulk modulus, K, so that the compressional velocity is $v_p = \sqrt{\frac{K}{\rho}} = \sqrt{\frac{\lambda}{\rho}}$.

If we define the actual c_{ijmn} from the elements of C, plug them back into the fully anisotropic Equation 2-26, we see that $u_1 = u_2 = u_3 = u$, and consequently that Equation 2-26 reduces to Equation 2-30, which is, of course, the normal three-dimensional scalar wave equation.

(2-30)
$$\frac{\partial^2 u}{\partial t^2} = \frac{\lambda}{\rho}\left(\frac{\partial^2 u}{\partial x_1^2} + \frac{\partial^2 u}{\partial x_2^2} + \frac{\partial^2 u}{\partial x_3^2}\right)$$

Equation 2-23 shows that $\tau_{i,j} = 0, i \neq j$, $\tau_{1,1} = \tau_{2,2} = \tau_{3,3} = \tau$, and $u_1 = u_2 = u_3 = u$, so that Equation 2-30 becomes Equation 2-31.

(2-31)
$$\begin{aligned} \frac{\partial^2 u}{\partial t^2} &= \frac{\lambda}{\rho}\left[\frac{\partial \tau}{\partial x_1} + \frac{\partial \tau}{\partial x_2} + \frac{\partial \tau}{\partial x_3}\right] \\ \tau &= \frac{\lambda}{\rho}\left[\frac{\partial u}{\partial x_1} + \frac{\partial u}{\partial x_2} + \frac{\partial u}{\partial x_3}\right] \end{aligned}$$

These two equations can also be written in first order form as Equation 2-32.

(2-32)
$$\begin{aligned} \frac{\partial v}{\partial t} &= \frac{\lambda}{\rho}\left[\frac{\partial \tau}{\partial x_1} + \frac{\partial \tau}{\partial x_2} + \frac{\partial \tau}{\partial x_3}\right] \\ \frac{\partial \tau}{\partial t} &= \frac{\lambda}{\rho}\left[\frac{\partial u}{\partial x_1} + \frac{\partial u}{\partial x_2} + \frac{\partial u}{\partial x_3}\right] \end{aligned}$$

Isotropic Elastic Symmetry

For isotropic elastic models, the C matrix takes the form in Equation 2-33, where μ is the second of the two Lamè parameters, and represents the shear modulus.

(2-33)
$$C = [c_{kl}] = \begin{bmatrix} \lambda+2\mu & \lambda & \lambda & 0 & 0 & 0 \\ \lambda & \lambda+2\mu & \lambda & 0 & 0 & 0 \\ \lambda & \lambda & \lambda+2\mu & 0 & 0 & 0 \\ 0 & 0 & 0 & \mu & 0 & 0 \\ 0 & 0 & 0 & 0 & \mu & 0 \\ 0 & 0 & 0 & 0 & 0 & \mu \end{bmatrix}$$

In this case, $v_p = \sqrt{\frac{\lambda+2\mu}{\rho}} = \sqrt{\frac{K+4\mu/3}{\rho}}$, and the shear velocity is then $v_s = \sqrt{\frac{\mu}{\rho}}$.

It is clear from these relationships, that given density, ρ, compressional velocity, v_p, and shear velocity, v_s, it is quite easy to solve for the coefficients in the C matrix, and then produce the propagation equation for synthesizing isotropic elastic seismic data. It is also

clear that modeling with this level of complexity is considerably more computationally intensive than is the case for acoustic models.

Given the matrix in Equation 2-33 and then using Equation 2-23 and Equation 2-25, we can write Equation 2-34.

(2-34)
$$
\begin{aligned}
\frac{\partial^2 u_1}{\partial t^2} &= \frac{1}{\rho}\left(\frac{\partial \tau_{1,1}}{\partial x_1} + \frac{\partial \tau_{1,2}}{\partial x_2} + \frac{\partial \tau_{1,3}}{\partial x_3}\right) \\
\frac{\partial^2 u_2}{\partial t^2} &= \frac{1}{\rho}\left(\frac{\partial \tau_{2,1}}{\partial x_1} + \frac{\partial \tau_{2,2}}{\partial x_2} + \frac{\partial \tau_{2,3}}{\partial x_3}\right) \\
\frac{\partial^2 u_3}{\partial t^2} &= \frac{1}{\rho}\left(\frac{\partial \tau_{3,1}}{\partial x_1} + \frac{\partial \tau_{3,2}}{\partial x_2} + \frac{\partial \tau_{3,3}}{\partial x_3}\right) \\
\tau_{1,1} &= \frac{\lambda + 2\mu}{\rho}\frac{\partial u_1}{\partial x_1} + \frac{\lambda}{\rho}\frac{\partial u_2}{\partial x_2} + \frac{\lambda}{\rho}\frac{\partial u_3}{\partial x_3} \\
\tau_{1,2} &= \frac{\mu}{\rho}\left(\frac{\partial u_1}{\partial x_2} + \frac{\partial u_2}{\partial x_1}\right) \\
\tau_{1,3} &= \frac{\mu}{\rho}\left(\frac{\partial u_1}{\partial x_3} + \frac{\partial u_3}{\partial x_1}\right) \\
\tau_{2,2} &= \frac{\lambda}{\rho}\frac{\partial u_1}{\partial x_1} + \frac{\lambda + 2\mu}{\rho}\frac{\partial u_2}{\partial x_2} + \frac{\lambda}{\rho}\frac{\partial u_3}{\partial x_3} \\
\tau_{2,3} &= \frac{\mu}{\rho}\left(\frac{\partial u_3}{\partial x_2} + \frac{\partial u_2}{\partial x_3}\right) \\
\tau_{3,3} &= \frac{\lambda}{\rho}\frac{\partial u_1}{\partial x_1} + \frac{\lambda}{\rho}\frac{\partial u_2}{\partial x_2} + \frac{\lambda + 2\mu}{\rho}\frac{\partial u_3}{\partial x_3}
\end{aligned}
$$

Note that each $\tau_{i,j}$ is expressed in terms of various partial derivatives of the u_i. Back substitution of these expressions into the formulas in Equation 2-34 for the second order time derivatives allows us to write the elastic particle displacement equation in the form of Equation 2-35.

(2-35)
$$
\frac{\partial^2 \mathbf{u}}{\partial t^2} = \left(\frac{\lambda + 2\mu}{\rho}\right)\nabla(\nabla \cdot \mathbf{u}) - \frac{\mu}{\rho}\nabla \times \nabla \times \mathbf{u}
$$

From a practical point of view, Equation 2-35 says that, even in the elastic case, we can solve for the vector components of particle displacement **u** in much the same way that we solve for the non-vector wavefield, u, in a scalar wave equation.

We can also write Equation 2-34 as a first order vector system. If we take the partial derivatives of the stress-strain terms, τ, in Equation 2-34 and let $v_i = \frac{\partial u_i}{\partial t}$, we obtain the

first order equation for particle velocity, Equation 2-36.

$$
\begin{aligned}
\frac{\partial v_1}{\partial t} &= \frac{1}{\rho}\left(\frac{\partial \tau_{1,1}}{\partial x_1} + \frac{\partial \tau_{1,2}}{\partial x_2} + \frac{\partial \tau_{1,3}}{\partial x_3}\right) \\
\frac{\partial v_2}{\partial t} &= \frac{1}{\rho}\left(\frac{\partial \tau_{2,1}}{\partial x_1} + \frac{\partial \tau_{2,2}}{\partial x_2} + \frac{\partial \tau_{2,3}}{\partial x_3}\right) \\
\frac{\partial v_3}{\partial t} &= \frac{1}{\rho}\left(\frac{\partial \tau_{3,1}}{\partial x_1} + \frac{\partial \tau_{3,2}}{\partial x_2} + \frac{\partial \tau_{3,3}}{\partial x_3}\right) \\
\frac{\partial \tau_{1,1}}{\partial t} &= \frac{\lambda + 2\mu}{\rho}\frac{\partial v_1}{\partial x_1} + \frac{\lambda}{\rho}\frac{\partial v_2}{\partial x_2} + \frac{\lambda}{\rho}\frac{\partial v_3}{\partial x_3} \\
\frac{\partial \tau_{1,2}}{\partial t} &= \frac{\mu}{\rho}\left(\frac{\partial v_1}{\partial x_2} + \frac{\partial v_2}{\partial x_1}\right) \\
\frac{\partial \tau_{1,3}}{\partial t} &= \frac{\mu}{\rho}\left(\frac{\partial v_1}{\partial x_3} + \frac{\partial v_3}{\partial x_1}\right) \\
\frac{\partial \tau_{2,2}}{\partial t} &= \frac{\lambda}{\rho}\frac{\partial v_1}{\partial x_1} + \frac{\lambda + 2\mu}{\rho}\frac{\partial v_2}{\partial x_2} + \frac{\lambda}{\rho}\frac{\partial v_3}{\partial x_3} \\
\frac{\partial \tau_{2,3}}{\partial t} &= \frac{\mu}{\rho}\left(\frac{\partial v_2}{\partial x_3} + \frac{\partial v_3}{\partial x_2}\right) \\
\frac{\partial \tau_{3,3}}{\partial t} &= \frac{\lambda}{\rho}\frac{\partial v_1}{\partial x_1} + \frac{\lambda}{\rho}\frac{\partial v_2}{\partial x_2} + \frac{\lambda + 2\mu}{\rho}\frac{\partial v_3}{\partial x_3}
\end{aligned}
\tag{2-36}
$$

Equation 2-36 provides a first order system of equations (in time) as opposed a second order system like that in Equation 2-26. Note that, because of symmetry, we need not write down the terms $\frac{\partial \tau_{2,1}}{\partial t} = \frac{\partial \tau_{1,2}}{\partial t}$, $\frac{\partial \tau_{3,1}}{\partial t} = \frac{\partial \tau_{1,3}}{\partial t}$, or $\frac{\partial \tau_{3,2}}{\partial t} = \frac{\partial \tau_{2,3}}{\partial t}$.

We can write Equation 2-36 in the form of Equation 2-37, where $\mathbf{S}(t)$ is a suitable vector source term, $\mathbf{v} = \left[v_1, v_2, v_3, \tau_{1,1}, \tau_{1,2}, \tau_{1,3}, \tau_{2,2}, \tau_{2,3}, \tau_{3,3}\right]^T$, and Equation 2-38 defines $\mathbf{H}$. The $\mathbf{A}$, $\mathbf{B}$, and $\mathbf{C}$ matrices in Equation 2-38 are themselves defined in Equation 2-39, Equation 2-40 and Equation 2-41, respectively.

$$
\frac{\partial \mathbf{v}}{\partial t} = \mathbf{H}\mathbf{v} + \mathbf{S} \tag{2-37}
$$

$$
\mathbf{H} = \mathbf{A}\frac{\partial \mathbf{v}}{\partial x_1} + \mathbf{B}\frac{\partial \mathbf{v}}{\partial x_2} + \mathbf{C}\frac{\partial \mathbf{v}}{\partial x_3} \tag{2-38}
$$

(2-39)
$$\mathbf{A} = \begin{bmatrix} 0 & 0 & 0 & \rho^{-1} & 0 & 0 & 0 & 0 & 0 \\ 0 & 0 & 0 & 0 & \rho^{-1} & 0 & 0 & 0 & 0 \\ 0 & 0 & 0 & 0 & 0 & \rho^{-1} & 0 & 0 & 0 \\ \frac{\lambda+2\mu}{\rho} & 0 & 0 & 0 & 0 & 0 & 0 & 0 & 0 \\ 0 & \frac{\mu}{\rho} & 0 & 0 & 0 & 0 & 0 & 0 & 0 \\ 0 & 0 & \frac{\mu}{\rho} & 0 & 0 & 0 & 0 & 0 & 0 \\ \frac{\lambda}{\rho} & 0 & 0 & 0 & 0 & 0 & 0 & 0 & 0 \\ 0 & 0 & 0 & 0 & 0 & 0 & 0 & 0 & 0 \\ \frac{\lambda}{\rho} & 0 & 0 & 0 & 0 & 0 & 0 & 0 & 0 \end{bmatrix}$$

(2-40)
$$\mathbf{B} = \begin{bmatrix} 0 & 0 & 0 & 0 & \rho^{-1} & 0 & 0 & 0 & 0 \\ 0 & 0 & 0 & 0 & 0 & 0 & \rho^{-1} & 0 & 0 \\ 0 & 0 & 0 & 0 & 0 & 0 & 0 & \rho^{-1} & 0 \\ 0 & \frac{\lambda}{\rho} & 0 & 0 & 0 & 0 & 0 & 0 & 0 \\ \frac{\mu}{\rho} & 0 & 0 & 0 & 0 & 0 & 0 & 0 & 0 \\ 0 & 0 & 0 & 0 & 0 & 0 & 0 & 0 & 0 \\ 0 & \frac{\lambda+2\mu}{\rho} & 0 & 0 & 0 & 0 & 0 & 0 & 0 \\ 0 & 0 & \frac{\mu}{\rho} & 0 & 0 & 0 & 0 & 0 & 0 \\ 0 & \frac{\lambda}{\rho} & 0 & 0 & 0 & 0 & 0 & 0 & 0 \end{bmatrix}$$

(2-41)
$$\mathbf{C} = \begin{bmatrix} 0 & 0 & 0 & 0 & 0 & \rho^{-1} & 0 & 0 & 0 \\ 0 & 0 & 0 & 0 & 0 & 0 & 0 & \rho^{-1} & 0 \\ 0 & 0 & 0 & 0 & 0 & 0 & 0 & 0 & \rho^{-1} \\ 0 & 0 & \frac{\lambda}{\rho} & 0 & 0 & 0 & 0 & 0 & 0 \\ 0 & 0 & 0 & 0 & 0 & 0 & 0 & 0 & 0 \\ \frac{\mu}{\rho} & 0 & 0 & 0 & 0 & 0 & 0 & 0 & 0 \\ 0 & 0 & \frac{\lambda}{\rho} & 0 & 0 & 0 & 0 & 0 & 0 \\ 0 & \frac{\mu}{\rho} & 0 & 0 & 0 & 0 & 0 & 0 & 0 \\ 0 & 0 & \frac{\lambda+2\mu}{\rho} & 0 & 0 & 0 & 0 & 0 & 0 \end{bmatrix}$$

Equation 2-38 is appealing because it is a one-dimensional, time-domain differential system whose solution is easily expressed as Equation 2-42, where $\mathbf{v}(0)$ represents the initial conditions. When we discuss numerical approximations to this equation, we will find this fact quite useful. It allows us to propagate wavefields one time stamp at a time without having to solve a second order system. It is also easily manipulated to produce a very efficient and accurate forward marching algorithm, the *evolution equation*.

(2-42)
$$\mathbf{v}(t) = e^{t\mathbf{H}}\mathbf{v}(0) + \int_0^t e^{\xi\mathbf{H}}\mathbf{S}(t-\xi)d\xi$$

Before developing the forward marching algorithm, we continue our discussion of the various types of data we might wish to synthesize.

Vertical Transverse Isotropy (VTI) Symmetry

The C matrix in Equation 2-43 defines what has become known as vertical transverse isotropy (VTI).

$$C = [c_{kl}] = \begin{bmatrix} c_{11} & c_{11}-2c_{66} & c_{13} & 0 & 0 & 0 \\ c_{11}-2c_{66} & c_{11} & c_{13} & 0 & 0 & 0 \\ c_{13} & c_{13} & c_{33} & 0 & 0 & 0 \\ 0 & 0 & 0 & c_{44} & 0 & 0 \\ 0 & 0 & 0 & 0 & c_{44} & 0 \\ 0 & 0 & 0 & 0 & 0 & c_{66} \end{bmatrix} \tag{2-43}$$

Waves propagating in media of this type exhibit a symmetry around the vertical or depth axis, z. Note that the pattern of this matrix is identical to that of the isotropic elastic C matrix. In fact, by setting $c_{11} = c_{33}$, $c_{44} = c_{55} = \mu$, and $c_{13} = \lambda$, the VTI C matrix becomes the isotropic elastic matrix. As we will see, the square roots of the ratios $\frac{c_{33}}{\rho}$ and $\frac{c_{44}}{\rho}$ specify the vertical compressional and shear velocities in the anisotropic medium. It should not be a surprise that the c_{ij} values in the matrix can be related to intuitive parameters more representative of how we think of the Earth.

We could again follow the development of Equation 2-36 to produce an equivalent for VTI media, but that is left to the reader. The important thing to notice is that implementation of a discrete version of the resulting first order system will almost certainly follow along the same lines as that for the isotropic elastic case above.

Rock types exhibiting VTI behavior include shales and thin-bed sequences.

Polar Isotropy Symmetry

The difference between VTI and polar isotropy is that the symmetry axis is tilted relative to the vertical axis. Early on, this type of anisotropic symmetry was called tilted transversely isotropic (TTI) anisotropy, but in this book I prefer to use Leon Thomsen's more general term, *polar symmetry*. Symmetry of this type is easily obtained by simply rotating the tensor c_{ijmn} of a VTI medium through a fixed angle. The new resulting C matrix produces wavefields that are symmetric around the new symmetry axis. In this case the axis can be relative to any plane through the medium and the propagation is symmetric relative to that plane. Unfortunately, when the symmetry axis is not aligned along the primary axis, neither the C matrix nor the tensor, c_{ijmn}, is particularly simple and generally does not have an easily recognized pattern. This may not be much of an issue since, when the rotation angle is known, it is possible to rotate back forth between VTI and TTI at any time.

Rock types with polar isotropy are identical to those exhibiting VTI, but in this case the symmetry is orthogonal to the dip of the rock.

Orthorhombic Isotropy Symmetry

Polar anisotropy, including VTI, is always defined by five parametric volumes and the two angles defining the symmetry axis. The C matrix with nine elements in Equation 2-44 defines orthorhombic anisotropy.

(2-44)
$$C = [c_{kl}] = \begin{bmatrix} c_{11} & c_{12} & c_{13} & 0 & 0 & 0 \\ c_{12} & c_{22} & c_{23} & 0 & 0 & 0 \\ c_{13} & c_{23} & c_{33} & 0 & 0 & 0 \\ 0 & 0 & 0 & c_{44} & 0 & 0 \\ 0 & 0 & 0 & 0 & c_{55} & 0 \\ 0 & 0 & 0 & 0 & 0 & c_{66} \end{bmatrix}$$

Orthorhombic anisotropy is probably the most realistic anisotropy that we will be able to handle or even use in the forceable future. Again, derivation of a first order system like that in Equation 2-26 is left to your discretion.

Examples of rock types that exhibit orthorhombic symmetry include

- thin-bed sequences or shale with a single set of vertical fractures
- isotropic formation with a single set of vertical, noncircular fractures
- thin-bed sequence, or shale, or a massive isotropic sandstone with orthogonal sets of vertical fractures

Thomsen Parameters

In the mid 1980's, Leon Thomsen's research into anisotropy at AMOCO's Tulsa, Oklahoma research lab lead him to define a collection of parameters that provided a much more intuitive picture of the entries in the C matrix. Thomsen began by defining Equation 2-45.

$$\begin{aligned} v_{P0} &= \sqrt{\frac{c_{33}}{\rho}} \\ v_{S0} &= \sqrt{\frac{c_{44}}{\rho}} \\ \varepsilon &= \frac{c_{11}-c_{33}}{2c_{33}} \\ \delta &= \frac{(c_{13}+c_{44})^2-(c_{33}-c_{44})^2}{2c_{33}(c_{33}-c_{44})} \\ \gamma &= \frac{c_{66}-c_{44}}{2c_{44}} \end{aligned} \tag{2-45}$$

He then showed that the exact plane wave velocities could be expressed as a function of the propagation angle, θ, using Equation 2-46, where D' is defined by Equation 2-47.

$$\begin{aligned} v_p^2(\theta) &= v_{P0}^2\left[1+\varepsilon\sin^2\theta + D'\right] \\ v_{s_\perp}^2(\theta) &= v_{S0}^2\left[1+\varepsilon\frac{v_{P0}^2}{v_{S0}^2}\sin^2\theta + \frac{v_{P0}^2}{v_{S0}^2}D'\right] \\ v_{s_\parallel}^2(\theta) &= v_{S0}^2\left[1+2\gamma\sin^2\theta\right] \end{aligned} \tag{2-46}$$

$$D' = \frac{(1-\frac{v_{S0}^2}{v_{S0}^2})}{2}\left[\left\{1+\frac{4(2\delta-\varepsilon)}{1-\frac{v_{S0}^2}{v_{S0}^2}}\sin^2\theta\cos^2\theta+\frac{4(1-\frac{v_{S0}^2}{v_{S0}^2}+\varepsilon)\varepsilon}{1-\frac{v_{S0}^2}{v_{S0}^2}}\sin^4\theta\right\}^{1/2}-1\right] \tag{2-47}$$

While these formulas have found considerable use for describing anisotropic models and for providing propagating equations for synthesis of anisotropic seismic data, the parameters of most importance for this book are the vertical and horizontal velocities. Typically, these velocities are defined from the *weak polar anisotropy* expressions in Equation 2-48 with values defined by Equation 2-49.

$$\begin{aligned} v_p^2(\theta) &\approx v_{P0}^2\left[1+\delta\sin^2\theta\cos^2\theta+\varepsilon\sin^4\theta\right] \\ v_{s_\perp}^2(\theta) &\approx v_{S0}^2\left[1+\frac{v_{P0}^2}{v_{S0}^2}(\varepsilon-\delta)\sin^2\theta\cos^2\theta\right] \\ v_{s_\parallel}^2(\theta) &\approx v_{S0}^2\left[1+2\gamma\sin^2\theta\right] \end{aligned} \tag{2-48}$$

(2-49)
$$\begin{array}{rcl} v_p(0^\circ) & \approx & v_{P0} \\ v_p(90^\circ) & \approx & v_{P0}(1+\varepsilon) \\ v_{s_\perp}(0^\circ) & \approx & v_{S0} \\ v_{s_\perp}(90^\circ) & \approx & v_{S0} \\ v_{s_\parallel}(0^\circ) & \approx & v_{S0} \\ v_{s_\parallel}(90^\circ) & \approx & v_{S0}(1+\gamma) \end{array}$$

Clearly, ε controls the percentage of anisotropy. It determines the speed of the horizontal velocity relative to the vertical velocity v_{S0}. What will become apparent as we progress through this book is that δ controls what I will refer to as *conversion to depth*.

Expressing anisotropic parameters in this manner provides a more natural idea of the parameters defining a polar anisotropic model. While there are many possible variations, such models are defined by four volumes, the vertical velocities v_{P0} and v_{S0}, ε, and δ. Equation 2-26 is then discretized to provide the necessary propagating equation.

Algorithms

Algorithms for synthesizing seismic data abound. Here we will focus on four such methods: Ray-based, finite-difference, finite-element, and Fourier-domain-based methods. Of course, you can construct algorithms in various combinations of these domains, so it is technically possible to develop approaches that work with finite-differences in frequency-space or even perhaps time and spatial frequency. Once the basic concepts for the four are fully developed, pursuing alternative domain combinations is relative straightforward.

To keep the discussion as simple as possible we will focus all of our attention on the two-dimensional versions of Equation 2-17, and the coupled system Equation 2-36.

Variational Formulation and Finite Elements

We begin with Equation 2-18 in the frequency domain, where $g(\vec{x}_s)$ is a pressure source located at $\vec{x}_s = (x_s, y_s, z_s)$, and with $\vec{x} = (x, y, z)$, $k(\vec{x}) = \frac{\omega}{v(\vec{x})}$.

Equation 2-50 has the variational form in Equation 2-51, where V is an element of a suitable space, $\mathscr{V}$, of functions that can be used to approximate $U(\vec{x})$.

(2-50)
$$\frac{k^2}{\rho}U(x,y,z,\omega) + \nabla \cdot \frac{1}{\rho}\nabla U = -g(x_s, y_s, z_s, \omega)$$

(2-51) $$\varphi(U,V) = \int_\Omega \frac{k^2}{\rho} UV d\Omega + \int_\Omega \frac{1}{\rho} \nabla U \cdot \nabla V d\Omega = -\int_\Omega g(\vec{x}_s, t) d\Omega$$

Given a family, V_k, of basis functions spanning $\mathscr{V}$, we can approximate U and g by Equation 2-52 and Equation 2-53, respectively.

(2-52) $$U(\vec{x}) = \sum_{k=1}^{n} A_k V_k(\vec{x})$$

(2-53) $$g(\vec{x}_s, \omega) = \sum_{k=1}^{n} b_k V_k(\vec{x})$$

Thus, the variational form in Equation 2-51 can be expressed in matrix form as Equation 2-54 or Equation 2-55, where $\vec{A}^T = [A_1, A_2, \ldots, A_n]$ and $\vec{b}^T = [b_1, b_2, \ldots, b_n]$.

(2-54) $$\sum_{k=1}^{n} A_k \varphi(V_k, V_j) = \sum_{k=1}^{n} b_k \int_\Omega V_k V_j d\Omega$$

(2-55) $$\mathbf{S}\vec{A} = \mathbf{M}\vec{b}$$

In this setting, **S** is called the *complex impedance matrix* and **M** is called the *stiffness matrix*. Note that we have dropped reference to frequency, ω, so that $\mathbf{S}\vec{A} = \mathbf{M}\vec{g}$ is a single frequency equation.

If we choose our discretization scheme properly, we may assume that **S** is square, symmetric, and invertible, so that the modeling operator $\mathbf{S}^{-1}$ generates data according to the formula in Equation 2-56.

(2-56) $$\vec{U} = \mathbf{S}^{-1}\vec{f}$$

The key point to this discussion is that we have wide latitude in the choice of V_k. We can divide the model into a collection of local regions and then define V_k through polynomials, pyramids, or perhaps even boxes over each of the sub domains. This approach works well when the problem is defined by things like bridges, aeronautical structures, and other rigid bodies, but has never gained ground in seismic settings.

Dividing the medium up in this way is quite difficult mathematically, so modern methods tend to choose uniformly square or rectangular domains. It is also convenient to have basis functions that are easily differentiable and orthogonal. Thus, in some sense,

the modern version of finite element methods (FEM) tends to look more and more like a very sophisticated finite difference approach. However you accomplish the model division, the need to invert a matrix of significant size remains a serious issue.

For example, consider the one dimensional case and define $V_k(x)$ using Equation 2-57.

(2-57)
$$V_k(x) = \begin{cases} \frac{x - x_{k-1}}{x_k - x_{k-1}} & x \in [x_{k-1}, x_k] \\ \frac{x_{k+1} - x_k}{x_{k+1} - x_k} & x \in [x_k, x_{k+1}] \\ 0 & elsewhere \end{cases}$$

As illustrated in Figure 2-11, the $V_k \ = \ 1, \ldots, n$ basis is composed of shifted and scaled tent functions. For the two-dimensional case, we again choose one basis function, V_k, per vertex, x_k, of the triangulation of the planar region Ω. The function V_k is the unique function of x whose value is 1 at x_k and zero at every $x_j, \ j \ \neq \ k$. This process extends easily to three dimensions.

Figure 2-11. Basis functions V_k (blue) and a linear combination of them, which is piecewise linear (red)

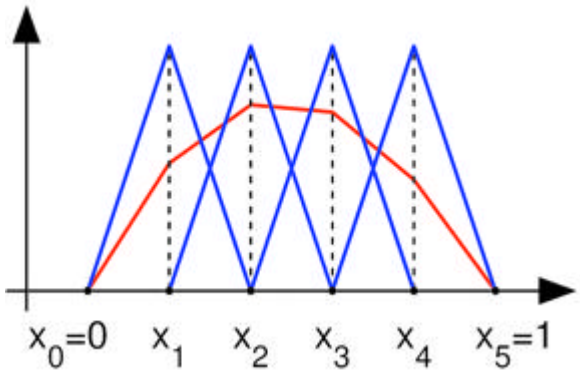

The primary advantage of this choice of basis is that the inner product in Equation 2-58 will be zero for almost all j, k.

(2-58)
$$\langle V_j, V_k \rangle = \int_0^1 V_j V_k \, dx$$

In the one dimensional case, the support of V_k is the interval $[x_{k-1}, x_{k+1}]$. Hence, the integrands of $\langle V_j, V_k \rangle$ and $\Phi(V_j, V_k)$ are identically zero whenever $|j - k| > 1$.

Similarly, in the planar case, if x_j and x_k do not share an edge of the triangulation, then the integrals 2-59 and 2-60 are both zero.

(2-59)
$$\int_\Omega V_j V_k \, ds$$

(2-60)
$$\int_{\Omega} \nabla V_j \cdot \nabla V_k \, ds$$

In two-dimensions, triangular elements can be used to approximate the domain of approximation in both regular and irregular ways. In Figure 2-12, a regular mesh is used to approximate the domain, and then through pyramids approximate the dome-like structure in the figure. Figure 2-12 illustrates a reasonably regular triangular decomposition of a domain at the bottom and the approximation to a dome accomplished through the use of the pyramidal versions of the basis functions in Figure 2-11. (From Wikipedia contributors,"Finite element method," Wikipedia, The Free Encyclopedia, http://en.wikipedia.org/w/index.php?title=Finite_element_method&oldid=298136444).

Figure 2-12. Domain triangles with pyramids as elements approximate a dome like surface. In this case the triangular basis mesh is regular. (From Wikipedia)

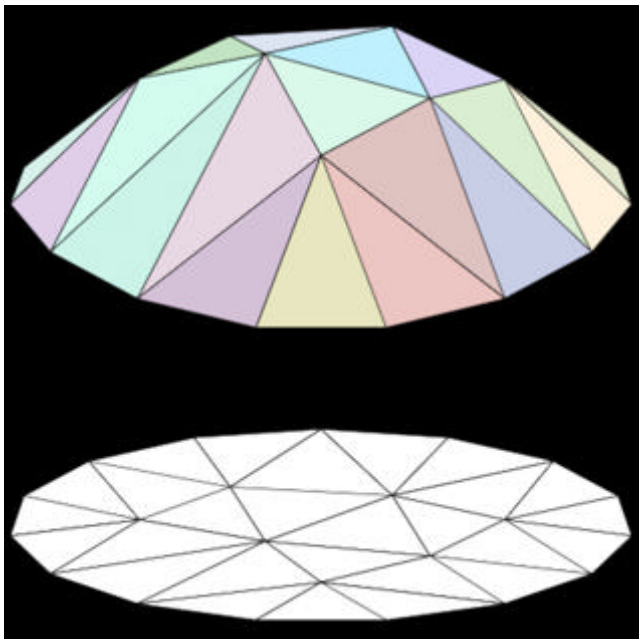

In contrast, Figure 2-13 shows an much more irregular approximation of the domain of approximation. It is an example of the utilization of irregularly sized triangles to decompose the domain of approximation. The mesh is denser in areas of interest.

Figure 2-13. Domain triangles with pyramids as elements approximate a dome like surface. Here the triangular basis mesh is irregular. (From Wikipedia)

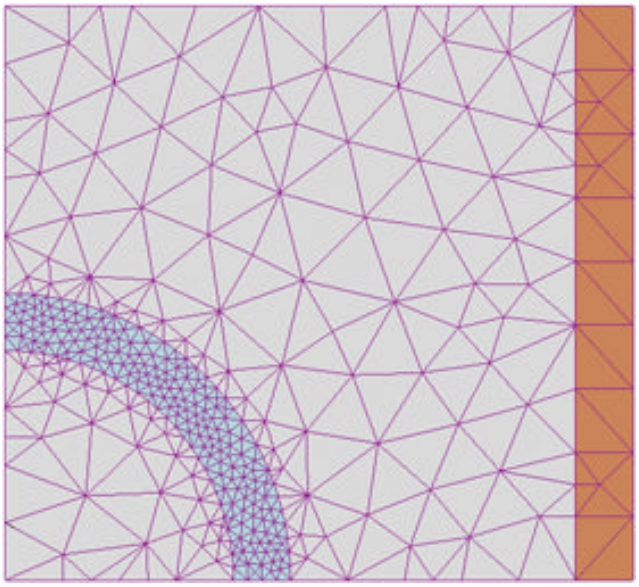

Figure 2-14 shows the general form of a 2D *S* matrix. Generally, this matrix has dimensions equal to the number of nodes or finite elements. An intriguing feature of the finite element method is that once the S-matrix is inverted, any and all shot responses can be synthesized from this single inverse.

Figure 2-14. The general form of the S-matrix in two-dimensions. (From Wikipedia)

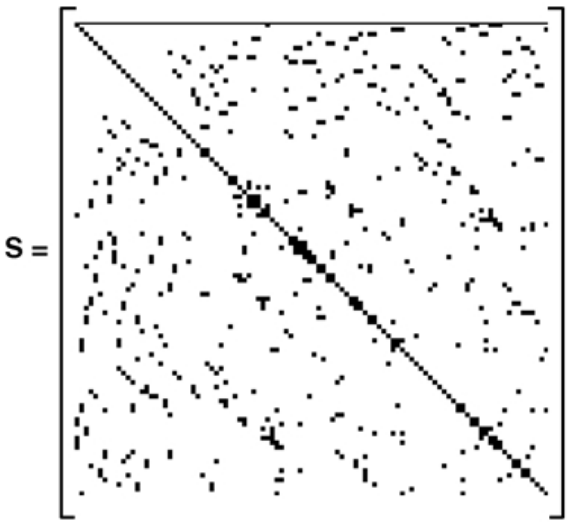

Depending on the author, the word “element” in “finite element method” refers either to the triangles in the domain, the piecewise linear basis function, or both. For our purposes, it is the latter. So, for instance, an author interested in curved domains might replace the triangles with curved primitives, in which case he might describe his elements as being curvilinear. On the other hand, some authors replace “piecewise linear” by “piecewise quadratic” or even “piecewise polynomial”. The author might then say “higher order element” instead of “higher degree polynomial”. The finite element method is not restricted to triangles (or tetrahedra in 3D, or higher order simplexes in multidimensional spaces), but can be defined on quadrilateral subdomains (hexahedra, prisms, or pyramids in 3D, and so on). Higher order shapes (curvilinear elements) can be defined with polynomial and even non-polynomial shapes (for example, ellipses or circles).

More advanced implementations (adaptive finite element methods) utilize a method to assess the quality of the results (based on error estimation theory) and modify the mesh during the solution, aiming to achieve an approximate solution within some bounds from the “exact” solution of the continuum problem. Mesh adaptivity may utilize various techniques, the most popular are:

- Moving nodes (r-adaptivity)
- Refining (and unrefining) elements (h-adaptivity)
- Changing order of base functions (p-adaptivity)
- Combinations of the above (hp-adaptivity)

In general, the finite element method is characterized by the following process.

- Choose a grid for Ω. In the preceding example the grid consisted of grid points or nodes, but one can also use triangles or curvilinear polygons.

- Choose basis functions. In our discussion, we used piecewise linear basis functions, but it is also common to use piecewise polynomial basis functions

A separate consideration is the smoothness of the basis functions. For second order elliptic boundary value problems, piecewise polynomial basis functions that are merely continuous will suffice (that is, the derivatives are discontinuous.) For higher order partial differential equations, you must use smoother basis functions. For instance, for a fourth order problem such as $u_{xxxx} + u_{yyyy} = f$, you can use piecewise quadratic basis functions that are both continuous and have first order derivatives.

An Old Movie

We can now use our modeling schema to generate synthetic shot data. Because we have a complete wavefield at each time step, we present the synthetic data in movie form. Our first movie (snapshots in Figure 2-15) was generated by R. G. Keys (now at ConocoPhillips in Houston, Texas) in February of 1982. At that time, the multiplicity of snapshots comprising these data required about 30 minutes to generate on a Cray 1S supercomputer. Today, almost any modern desktop, and even some laptops, can produce the same movie virtually in real time. As the movie progresses, please note that waves travel in all directions and the wavefield recorded at the top surface of this model would include refractions, reflections, and all forms of multiples.

Figure 2-15. Snapshot from 1982 Finite Element Pinchout Model synthesis.

Finite Differences

At first glance, finite difference modeling is by far the simplest method to grasp, since all that is necessary is to replace the continuous partial derivatives by discrete approximations. However, difficulty arises in producing an accurate approximation to the various derivatives. There are two generally accepted approaches to finding these approximations. The first is based purely on some form of fitting algorithm, frequently using polynomials, wherein a set of basis functions with known derivatives approximate the function whose derivative is required. Once the fit is obtained the derivative is defined in terms of the approximating functions.

The second way to approximate the derivatives is the finite element method (FEM). In FEM, the region of interest is divided into numerous connected subregions or elements within which approximate functions (usually polynomials) are used to represent the unknown quantity.

Polynomial Differences

The easiest approach to finite difference approximation is to simply use a difference quotient in Equation 2-61, like we did when we derived the full two-way equation. This is called a first order forward difference approximation.

(2-61)
$$\frac{du}{dx} = \frac{u(x + \Delta x) - u(x)}{\Delta x}$$

Similarly, we have the backward difference approximation in the form of Equation 2-62.

(2-62)
$$\frac{du}{dx} = \frac{u(x) - u(x - \Delta x)}{\Delta x}$$

What may not be clear is that these formulas are the result of approximating u by a straight line between $x + \Delta x$ and x and between $x - \Delta x$ and x.

One of the more popular methods for polynomial approximation is based on the Lagrange polynomial in Equation 2-63 defined for a sequence of points $[x_0, x_1, x_2, \ldots x_n]$.

(2-63)
$$L_{n,k}(x) = \prod_{\substack{i=0 \\ i \neq k}}^{i=n} \frac{(x - x_i)}{(x_k - x_i)}$$

Any function $f(x)$ can be defined such that the point sequence can then be approximated by the formula of Equation 2-64.

(2-64)
$$P(x) = \sum_{k=0}^{k=n} f(x_k) L_{n,k}(x)$$

Approximations to the derivatives of $f(x)$ can then be approximated through derivatives of the polynomial P. Since P will always be of the form in Equation 2-65, the approximate derivative will always be a weighted sum of the values of $f(x)$ at the sequence $[x_0, x_1, x_2, \ldots x_n]$.

(2-65) $$P(x) = a_0 + a_1 x + a_2 x^2 + \ldots a_n x^n$$

More accurate approximations can be obtained through the use of other polynomial bases, including the Hermite and Chebychev polynomials.

Taylor Series Differences

The Taylor series for $u(x \pm \Delta x)$ in terms of $u(x)$ is given in Equation 2-66.

(2-66) $$u(x \pm \Delta x) = u(x) \pm \frac{\partial u}{\partial x}\Delta x + \frac{\partial^2 u}{\partial x^2}\frac{\Delta x^2}{2!} \pm \frac{\partial^3 u}{\partial x^3}\frac{\Delta x^3}{3!} + \ldots$$

If we rearrange this series in the form Equation 2-67, we immediately recognize that the forward and backward differences are accurate to Δx. Mathematically, we say that the forward and backward differences are $O(\Delta x)$.

(2-67) $$\frac{u(x \pm \Delta x) - u(x)}{\Delta x} = \pm\frac{\partial u}{\partial x} + \frac{\partial^2 u}{\partial x^2}\frac{\Delta x}{2!} \pm \frac{\partial^3 u}{\partial x^3}\frac{\Delta x^2}{3!} + \ldots$$

The Taylor series in Equation 2-66 can easily form the basis for other more accurate formulas. The most obvious formula arises from the sum of the Taylor series expansions for $u(x + \Delta x) - u(x)$ and $u(x) - u(x - \Delta x)$. This immediately yields the central difference formula in Equation 2-68 which is $O(\Delta x^2)$.

(2-68) $$\frac{u(x + \Delta x) - u(x - \Delta x)}{2\Delta x} = \frac{\partial u}{\partial x} + \frac{\partial^3 u}{\partial x^3}\frac{\Delta x^2}{3!} + \frac{\partial^5 u}{\partial x^5}\frac{\Delta x^4}{5!} + \ldots$$

Since we generally think of Δx as being much less than 1 in magnitude, this central difference formula is clearly an improvement over a first-order forward or backward difference.

Second Order Differences

When we summed the formulas for $u(x + \Delta x) - u(x)$ and $u(x) - u(x - \Delta x)$, we obtained a series that contained odd order derivatives. Accordingly, if we subtract the two formulas, we obtain a series that contains only even order derivatives. This immediately produces the $O(\Delta x^2)$ formula for the second derivative with respect to x.

(2-69) $$\frac{u(x + \Delta x) - 2u(x) + u(x - \Delta x)}{\Delta x^2} = \frac{\partial u^2}{\partial x^2} + \frac{\partial^4 u}{\partial x^4}\frac{\Delta x^2}{4!} + \frac{\partial^6 u}{\partial x^6}\frac{\Delta x^4}{6!} + \ldots$$

High Order Differences

Extension of the second order central difference formula to higher orders is tedious but straight forward. For any given k (real or integer), there is Equation 2-70.

$$\frac{u(x+k\Delta x)+u(x-k\Delta x)}{2} = u(x)+k^2\frac{\partial u^2}{\partial x^2}\frac{\Delta x^2}{2!}+k^4\frac{\partial^4 u}{\partial x^4}\frac{\Delta x^4}{4!} + k^6\frac{\partial^6 u}{\partial x^6}\frac{\Delta x^6}{6!}+k^8\frac{\partial^8 u}{\partial x^8}\frac{\Delta x^8}{8!}+\ldots \tag{2-70}$$

Thus, if we want a fourth order scheme, we take the two terms in Equation 2-71 and Equation 2-72, solve the second term for the fourth order partial derivative and substitute the result into the first term to obtain Equation 2-73.

$$\frac{u(x+\Delta x)+u(x-\Delta x)}{2} = u(x)+\frac{\partial u^2}{\partial x^2}\frac{\Delta x^2}{2!}+\frac{\partial^4 u}{\partial x^4}\frac{\Delta x^4}{4!} \tag{2-71}$$

$$\frac{u(x+2\Delta x)+u(x-2\Delta x)}{2} = u(x)+4\frac{\partial u^2}{\partial x^2}\frac{\Delta x^2}{2!}+16\frac{\partial^4 u}{\partial x^4}\frac{\Delta x^4}{4!} \tag{2-72}$$

$$\frac{u(x+2\Delta x+16u(x+\Delta x)-34u(x)+16u(x-\Delta x)+u(x-2\Delta x)}{12\Delta x^2}\approx\frac{\partial u^2}{\partial x^2} \tag{2-73}$$

Higher order central difference approximations are obtained by simply adding additional terms to the mix. For example, a 10th order accurate term is obtained by back-substitution in the five equations when $k = 1,2,3,4,5$. The result is a scheme of the form in Equation 2-74, where the terms are given in Table 2.1.

$$\frac{\partial u^2}{\partial x^2}\approx\sum_{-5}^{5} w_k u(x-k\Delta x) \tag{2-74}$$

Table 2.1. Spatial Difference Terms

|k|	w
0	-5.8544444444
1	3.3333333333
2	-0.4761904762
3	0.0793650794
4	-0.0099206349
5	0.0006349206

Finite Differences for the Pressure Formulation

We can now formulate a finite difference propagation equation of just about any order we would like. However, it is of interest to reconsider the graphic in Figure 2-16(b). This figure, based on a simple second-order space-time difference equation shows that to compute any given fixed time stamp, the maximum extent of the stencil is exactly equal to three in each spatial direction and two in time. Thus, to make this process computationally efficient, it is prudent to keep the three $t - \Delta t$, t and $t + \Delta t$ volumes in memory at all times.

It is clear from Equation 2-74 that higher order differences will produce stencils with maximum extent determined by the maximum value of k. Thus, if we chose to use a 10th order scheme for each both space and time, our propagator will be 11 grid nodes wide in each spatial direction and 10 volumes in memory for each of the time stamps $t - k\Delta t$ for $k = -5, 5$. Even with current computational capabilities, holding this many volumes in memory is somewhat impractical. It is natural to try and find a procedure that avoids this memory explosion problem.

Graphical Descriptions

Figure 2-16(a) demonstrates two-dimensional propagation and Figure 2-16(b) demonstrates three-dimensional propagation in what is generally called acoustic Earth models. Note that the central difference stencil extends from time $t - \Delta t$ to time t to compute an output point at $t + \Delta t$.

Figure 2-16. Graphical interpretation of (a) 2-D and (b) 3-D propagators.

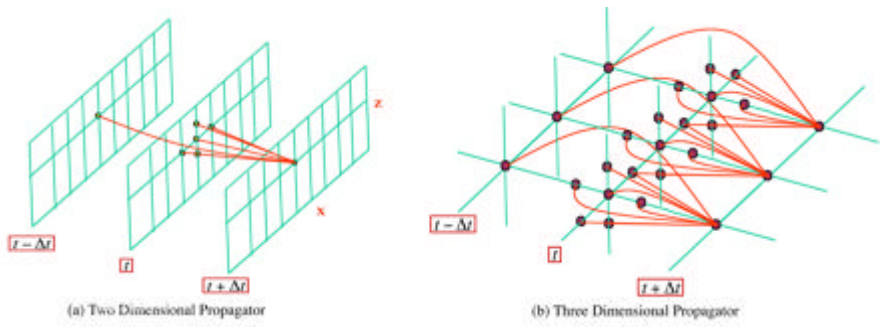

Note that in both cases, the stencil surrounds the ultimate output point to compute the new value. In the 2-D case, the stencil nodes are planar, while the 3-D nodes are volumetric. Thus, the wavefields are allowed to propagate upward, downward, and laterally in all directions as the propagation continues. It also means that we must compute all nodes at step t before we can compute any of the nodes at $t + \Delta t$. The examples in the last three figures produce what is called two-way propagation. All waveform styles (for example, refractions, free-surface, and peg-leg multiples) are possible in this setting since these propagators synthesize full waveform data.

Lax-Wendroff Method

Probably the best known "trick", initially published by Peter Lax and Burton Wendroff (see also M.A. Dablain), used the wave equation to find an accurate fourth order difference for $\frac{\partial^2}{\partial t^2}$ that does not increase the overall memory requirement. To understand this trick, consider the case in two dimensions when the velocity is constant and $\rho = 1$. From earlier efforts, we have Equation 2-75.

$$\begin{aligned} \frac{\partial^2 p}{\partial t^2} &= \frac{1}{\Delta t^2}\left(p(t+\Delta t) - 2p(t) + p(t-\Delta t) - \sum_{i=2}^{i=\infty} \frac{\partial^{2i} p}{\partial t^{2i}} \frac{\Delta t^{2i}}{2i!}\right) \\ &\approx \frac{1}{\Delta t^2}\left(p(t+\Delta t) - 2p(t) + p(t-\Delta t) - \frac{\partial^4 p}{\partial t^4} \frac{\Delta t^4}{12!}\right) \end{aligned} \tag{2-75}$$

We also know the second order derivative, $\frac{\partial^2 p}{\partial t^2}$, in Equation 2-76.

$$\frac{\partial^2 p}{\partial t^2} = v^2\left(\frac{\partial^2 p}{\partial x^2} + \frac{\partial^2 p}{\partial z^2}\right) \tag{2-76}$$

Thus, the fourth order derivative in time is given by Equation 2-77.

$$\begin{aligned} \frac{\partial^4 p}{\partial t^4} &= v^2\left[\frac{\partial^2 p}{\partial x^2}\left(\frac{\partial^2 p}{\partial t^2}\right) + \frac{\partial^2 p}{\partial z^2}\left(\frac{\partial^2 p}{\partial t^2}\right)\right] \\ &= v^2\left[\frac{\partial^2 p}{\partial x^2}\left(\frac{\partial^2 p}{\partial x^2} + \frac{\partial^2 p}{\partial z^2}\right) + \frac{\partial^2 p}{\partial z^2}\left(\frac{\partial^2 p}{\partial x^2} + \frac{\partial^2 p}{\partial z^2}\right)\right] \\ &= v^4\left(\frac{\partial^4 p}{\partial x^4} + 2\frac{\partial^4 p}{\partial x^2 \partial z^2} + \frac{\partial^4 p}{\partial x^4}\right) \end{aligned} \tag{2-77}$$

It should be noted that the assumptions of constant density and velocity are not necessary because the Lax-Wendroff scheme generalizes our scheme for finding higher order central difference terms through the recursive formula in Equation 2-78.

$$\frac{\partial^{2i} p}{\partial t^{2i}} = -\left(\rho v^2 \nabla \cdot \frac{1}{\rho} \nabla p\right) \frac{\partial^{2i-2} p}{\partial t^{2i-2}} \tag{2-78}$$

In this case, the higher order time derivatives can be computed from higher order spatial derivatives by applying the spatial side of the original wave equation.

If we now replace the spatial derivatives using formulas like that in Equation 2-74, we arrive at a fourth order formula for the second partial derivative in time. After

calculating all the various weights, replacing partial derivatives with central differences, and solving for $p_{i,j,n+1} = p(i\Delta x, j\Delta z, n\Delta t + \Delta t)$, we arrive at a discrete central difference formula of general form shown in Equation 2-79.

$$p_{i,j,n+1} = -2p_{i,j,n} + p_{i,j,n-1} + \Delta t^2 \left[v^4 \sum_k \sum_m a_{k,m} p_{i-k,j-m,n} + v^2 \left(\sum_k b_k p_{i-k,j,n} + \sum_m c_m p_{i,j-m,n} \right) \right] + s_{i_0,j_0,n} \quad (2\text{-}79)$$

For clarity, Δx^2 and Δy^2 have been suppressed, and $s_{i_0,j_0,n}$ represents a source at the location specified by i_0 and j_0.

Formulas of this kind are generally called *difference equations* and provide what is usually called an *explicit* forward marching algorithm for data synthesis. Schemes of this kind are also called *quadrature methods* because they are integrating the wave equation to synthesize a response to a given stimulus.

Figure 2-17 shows a simple pyramid model and data. The finite difference data over this model was synthesized on VAX 11-780 computers in late 1981 and early 1982. At that time, the calculations necessary to compute each shot required on the order of 48 hours. Today, most laptops can compute the entire set of 24 shots in minutes.

Figure 2-17. A simple pyramid model and data.

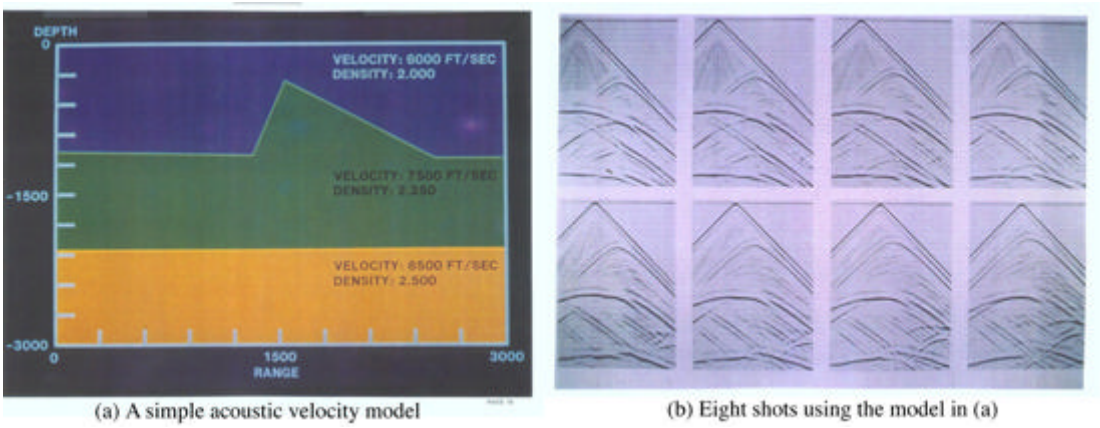

(a) A simple acoustic velocity model

(b) Eight shots using the model in (a)

Elastic Finite Differences

We now turn our attention to discrete simulation of vector elastic data. We can do this using either Equation 2-35 or Equation 2-36. Choosing the first equation leads to a method that is essentially the same as the pure explicit finite difference algorithm discussed in the previous section. To gain a slightly different perspective, we base our

formulation on Equation 2-36 and again we limit ourselves to the 2D case. In somewhat more familiar notation, Equation 2-36 becomes Equation 2-80.

$$
\begin{aligned}
\frac{\partial v_1}{\partial t} &= \rho^{-1}\left(\frac{\partial \tau_{1,1}}{\partial x_1} + \frac{\partial \tau_{1,2}}{\partial x_2}\right) \\
\frac{\partial v_2}{\partial t} &= \rho^{-1}\left(\frac{\partial \tau_{1,2}}{\partial x_1} + \frac{\partial \tau_{2,2}}{\partial x_2}\right) \\
\frac{\partial \tau_{1,1}}{\partial t} &= (\lambda + 2\mu)\frac{\partial v_1}{\partial x_1} + \lambda\frac{\partial v_2}{\partial x_2} \\
\frac{\partial \tau_{1,2}}{\partial t} &= \mu\left(\frac{\partial v_1}{\partial x_2} + \frac{\partial v_2}{\partial x_1}\right) \\
\frac{\partial \tau_{2,2}}{\partial t} &= \lambda\frac{\partial v_1}{\partial x_1} + (\lambda + 2\mu)\frac{\partial v_2}{\partial x_2}
\end{aligned}
\tag{2-80}
$$

We note that v_1 is the horizontal velocity and v_2 is the vertical velocity of a particle at any given position in space.

In this case, Equation 2-42 (the evolution equation) becomes Equation 2-81, where **v**, **H**, **A** and **B** are given by Equation 2-82 through Equation 2-85, respectively.

$$\frac{\partial \mathbf{v}}{\partial t} = \mathbf{H}\mathbf{v} + \mathbf{S} \tag{2-81}$$

$$\mathbf{v} = \left[v_1, v_2, \tau_{1.1}, \tau_{1,2}, \tau_{2,2}\right]^T \tag{2-82}$$

$$\mathbf{H} = \mathbf{A}\frac{\partial \mathbf{v}}{\partial x_1} + \mathbf{B}\frac{\partial \mathbf{v}}{\partial x_2} \tag{2-83}$$

$$\mathbf{A} = \begin{bmatrix} 0 & 0 & \rho^{-1} & 0 & 0 \\ 0 & 0 & 0 & \rho^{-1} & 0 \\ \lambda + 2\mu & 0 & 0 & 0 & 0 \\ 0 & \mu & 0 & 0 & 0 \\ \lambda & 0 & 0 & 0 & 0 \end{bmatrix} \tag{2-84}$$

$$\mathbf{B} = \begin{bmatrix} 0 & 0 & 0 & \rho^{-1} & 0 \\ 0 & 0 & 0 & 0 & \rho^{-1} \\ 0 & \lambda & 0 & 0 & 0 \\ \mu & 0 & 0 & 0 & 0 \\ 0 & \lambda + 2\mu & 0 & 0 & 0 \end{bmatrix} \tag{2-85}$$

Recall that the solution of Equation 2-81 has the form of Equation 2-86.

$$\mathbf{v}(t) = e^{t\mathbf{H}}\mathbf{v}(0) + \int_0^t e^{\tau\mathbf{H}}\mathbf{S}(t-\tau)d\tau \tag{2-86}$$

Equation 2-86 is immediately recognizable as a convolution in time. Thus, the progression from initial state to final state is really just a recursive convolution at each time stamp t. The well known series expansion for e^x provides an immediate approach to providing a discrete evolution equation for the solution vector $\mathbf{v}(t)$. The resulting scheme is equivalent to the Lax-Wendroff methodology and so will not be discussed further. If you are interested, you are encouraged to work out the mathematical details.

Staggered Grids

What we would like to develop is a finite difference solution to the system in Equation 2-81. We could, of course, use the higher order difference formulas developed through the use of the system in Equation 2-72. Several authors (Jean Virieux and A. Lavender) have suggested that somewhat higher accuracy might be achieved through the use of smaller time and space increments. Thus, their idea was to simply rewrite Equation 2-72 in the form of Equation 2-87 and Equation 2-88.

$$\frac{u(x+\frac{\Delta x}{2}) + u(x-\frac{\Delta x}{2})}{2} = u(x) + \frac{\partial u^2}{\partial x^2}\frac{\Delta x^2}{4\times 2!} + \frac{\partial^4 u}{\partial x^4}\frac{\Delta x^4}{16\times 4!} \tag{2-87}$$

$$\frac{u(x+\Delta x) + u(x-\Delta x)}{2} = u(x) + \frac{\partial u^2}{\partial x^2}\frac{\Delta x^2}{2!} + \frac{\partial^4 u}{\partial x^4}\frac{\Delta x^4}{4!} \tag{2-88}$$

This equation, of course, results in a difference formula of the form in Equation 2-89.

$$\frac{\partial^2 u}{\partial x^2} \approx \sum_{i=0}^{i=N} w_i u(x - \frac{i}{2}\Delta x) \tag{2-89}$$

Note that in Equation 2-89, the actual derivative is still estimated at a fixed grid point, but the accuracy is based on half the sampling increment.

At first glance, it might seem that a discrete solution of the system in Equation 2-80 using formulas based on half derivatives would require significantly more storage than using formulas defined at the normal sampling increments. However, it turns out that this is not the case if we first simplify the notation by defining $[v, w, \sigma, \xi, \zeta] = \left[v_1, v_2, \tau_{1,2}, \tau_{1,2}, \tau_{2,2}\right]$ so that we can then write $v_{i,j}^k = v_1(i\Delta x, j\Delta y, k\Delta t)$ for any sampling rate, and similarly for w, σ, ξ, and ζ.

A fourth order scheme in space and a second order scheme in time to solve Equation 2-80 can then be expressed as Equation 2-90.

$$v_{i,j}^{k+1/2} = v^{k-1/2} + \rho_{i,j}^{-1}\frac{\Delta t}{\Delta x}\left(\sigma_{i+1/2,j}^{k} - \sigma_{i-1/2,j}^{k}\right) + \rho_{i,j}^{-1}\frac{\Delta t}{\Delta z}\left(\sigma_{i,j+1/2}^{k} - \sigma_{i,j-1/2}^{k}\right)$$

$$w_{i+1/2,j+1/2}^{k+1/2} = w_{i+1/2,j+1/2}^{k-1/2} + \rho_{i+1/2,j+1/2}^{-1}\frac{\Delta t}{\Delta x}\left(\sigma_{i+1,j+1/2}^{k} - \sigma_{i,j+1/2}^{k}\right) + \rho_{i+1/2,j+1/2}^{-1}\frac{\Delta t}{\Delta z}\left(\zeta_{i+1/2,j+1}^{k} - \zeta_{i+1/2,j}^{k}\right)$$

(2-90)

$$\sigma_{i+1/2,j}^{k+1} = \sigma_{i+1/2,j}^{k} + \left(\lambda + 2\mu\right)_{i+1/2,j}\frac{\Delta t}{\Delta x}\left(v_{i+1,j}^{k+1/2} - v_{i,j}^{k+1/2}\right) + \lambda_{i+1/2,j}\frac{\Delta t}{\Delta z}\left(w_{i,j+1}^{k+1/2} - w_{i,j}^{k+1/2}\right)$$

$$\zeta_{i+1/2,j}^{k+1} = \zeta_{i+1/2,j}^{k} + \left(\lambda + 2\mu\right)_{i+1/2,j}\frac{\Delta t}{\Delta x}\left(w_{i+1,j}^{k+1/2} - w_{i,j}^{k+1/2}\right) + \lambda_{i+1/2,j}\frac{\Delta t}{\Delta z}\left(u_{i,j+1}^{k+1/2} - u_{i,j}^{k+1/2}\right)$$

$$\xi_{i,j+1/2}^{k+1} = \xi_{i,j+1/2}^{k} + \mu_{i,j+1/2}\frac{\Delta t}{\Delta z}\left(u_{i,j+1}^{k+1/2} - u_{i,j}^{k+1/2}\right) + \mu_{i,j+1/2}\frac{\Delta t}{\Delta x}\left(w_{i+1,j}^{k+1/2} - u_{i,j}^{k+1/2}\right)$$

The major difference between this and the usual sampling increment scheme is that the different components of the velocity field are not known at the same node. The actual size of each grid is identical to that of a more traditional equally spaced approach so staggering the grid does not change the overall size of the problem

Figure 2-18 and Figure 2-19 demonstrate staggered grid propagation graphically. The first of these figures show how the model parameters intermingle with data values at each grid node. The second figure shows how each stencil for each of the propagating wavefields is applied. Note that going from one time stamp to the next requires you to cycle through an application of four different stencils.

Figure 2-18. Distribution of variables and parameters (ρ, c_{ij}) in a 2D staggered grid mesh.

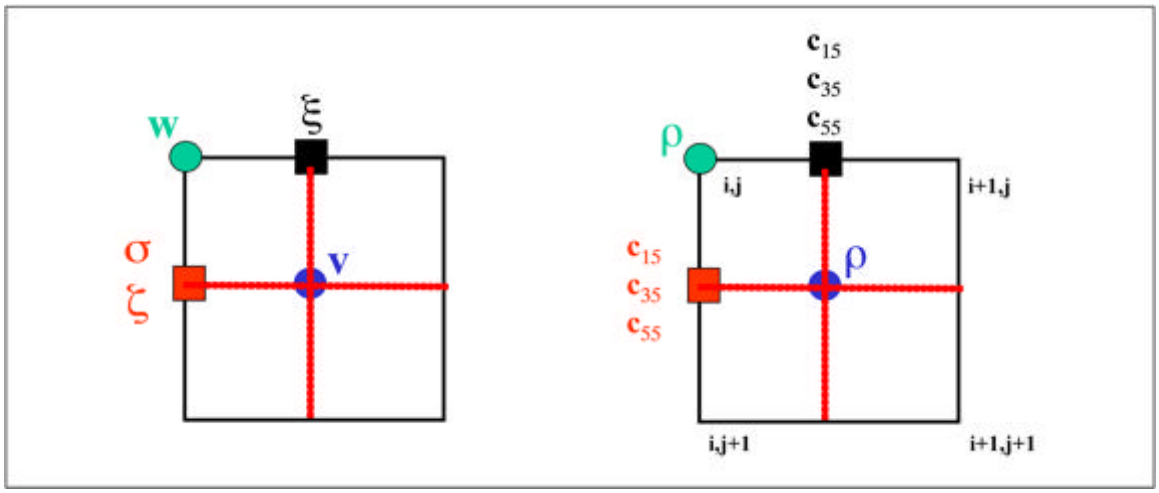

Figure 2-19. Staggered grid fnite difference stencils.

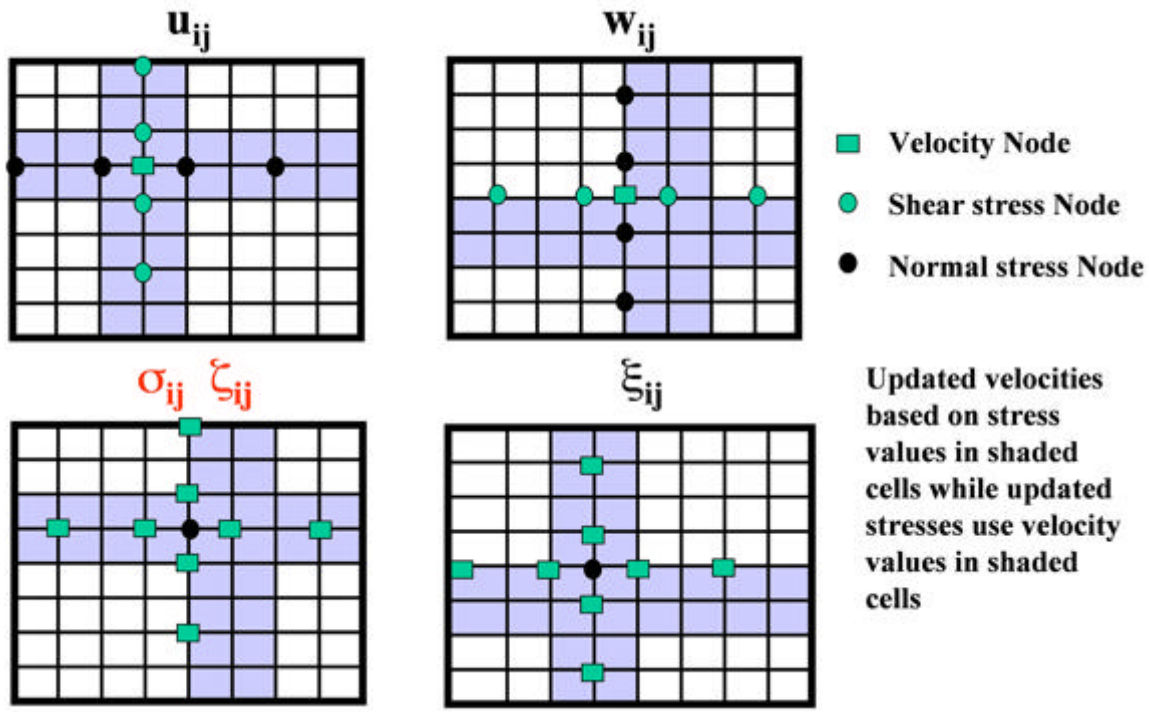

It is clear that synthesizing data over elastic models requires significantly more computational resources than when the model is acoustic. Simple isotropic elastic models are described by six volumes, while VTI and full elastic models require seven and eight volumes, respectively. In addition to this increase in storage, the computational load increases by at least one order of magnitude.

Figures 2-20 through 2-24 provide clear examples of simulations over both isotropic elastic and VTI models. Figure 2-20 illustrates an isotropic elastic version of the SEG/EAGE salt model along with representative inline compressional and shear responses. Figure 2-21 and Figure 2-22 show similar images over the Marmousi2 isotropic elastic model. Figure 2-23 and Figure 2-24 provide graphics of the full VTI model and VTI shot responses.

Figure 2-20. Isotropic elastic SEG/EAGE salt model with compressional and shear shot response.

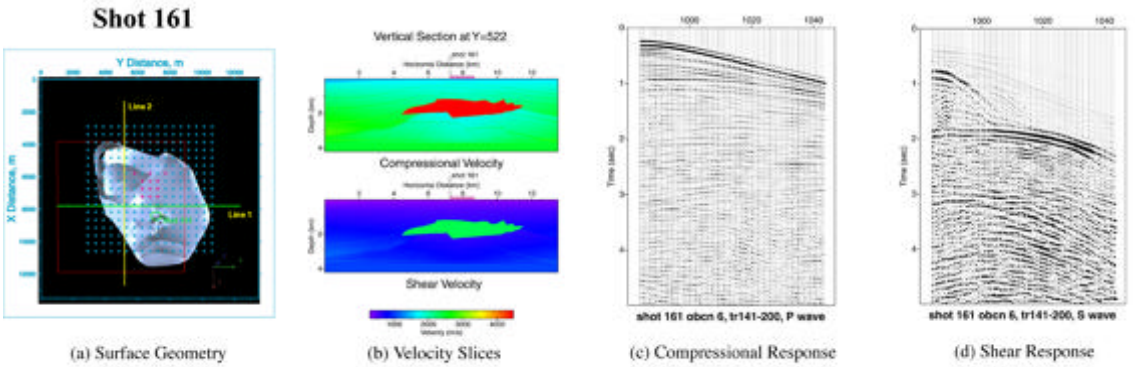

(a) Surface Geometry (b) Velocity Slices (c) Compressional Response (d) Shear Response

Figure 2-21. Marmousi2. Isotropic elastic version of the original Marmousi data.

(a). Compressional Velocity **(b).** Shear Velocity **(c).** Density

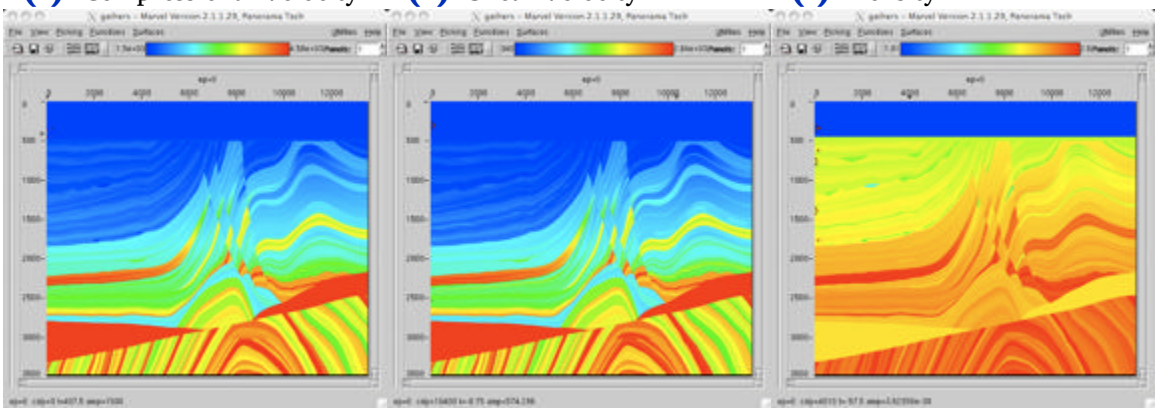

Figure 2-22. Marmousi2. Synthetic horizontal particle velocity and vertical particle velocity.

(a). Horizontal Shot-VSP **(b).** Vertical Shot-VSP

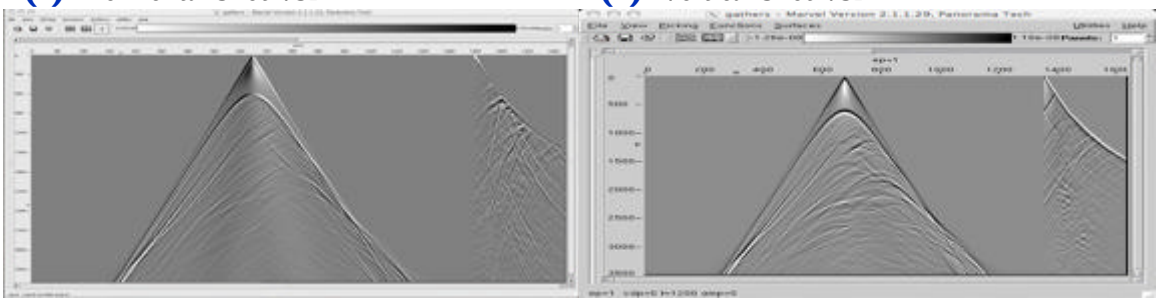

Figure 2-23. Hess Corporation VTI model. Available from the SEG.

(a). c11 **(b).** c13 **(c).** c33

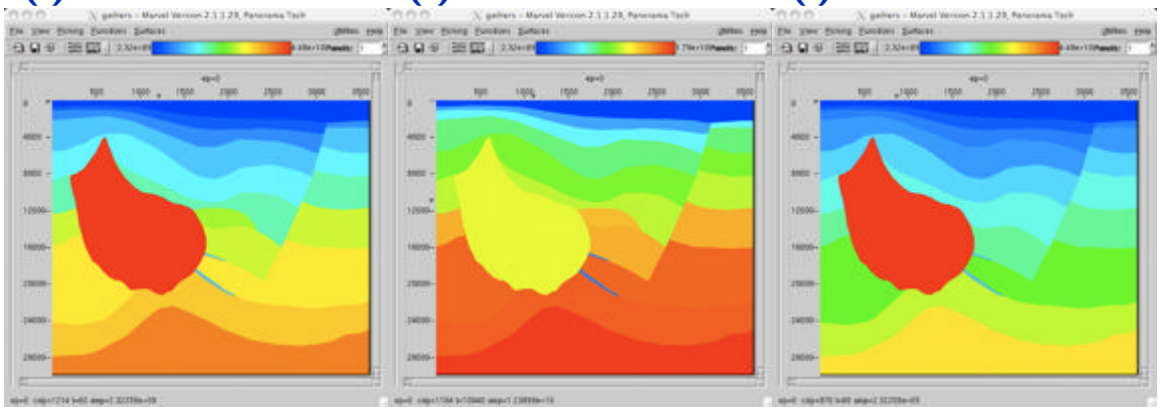

(d). c55 **(e).** Density

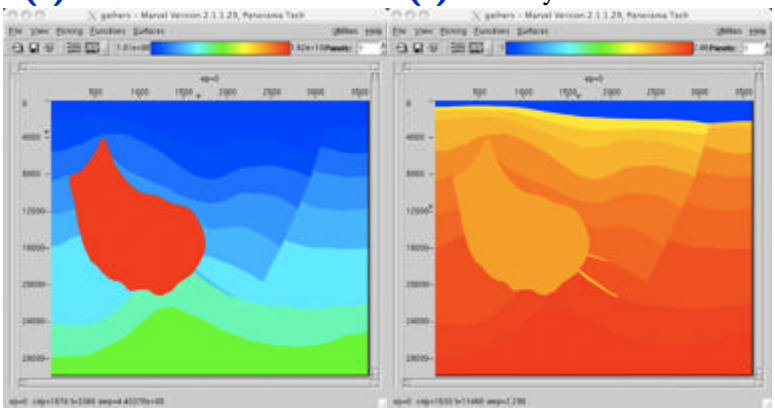

Figure 2-24. Hess-VTI. Synthetic Particle Velocities

(a). Horizontal Particle Velocity **(b).** Vertical Particle Velocity

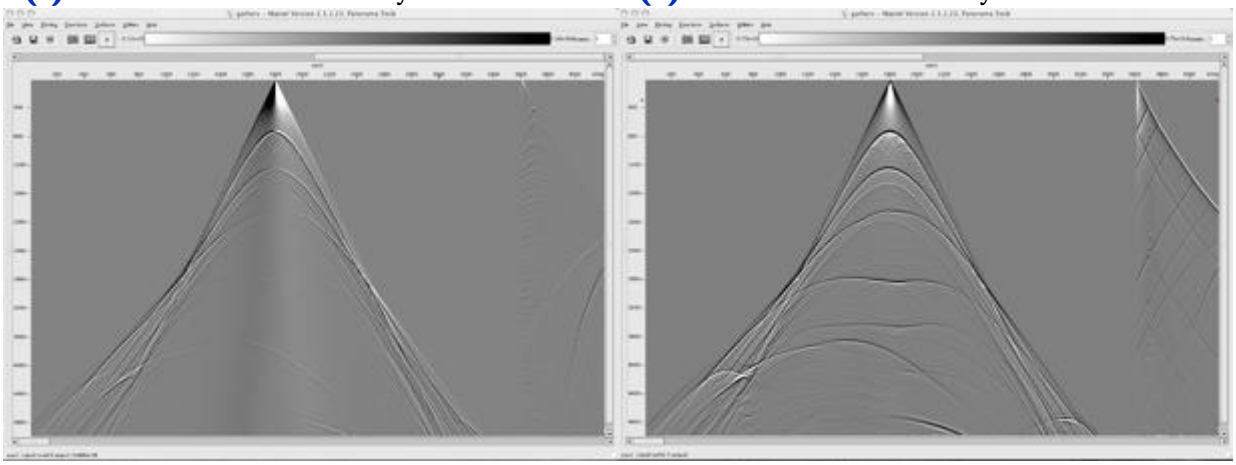

Predictor-Corrector Schemes

Equation 2-86 can be approximated by a first-order difference to produce the Euler or forward predictor scheme in Equation 2-91.

(2-91) $$\overline{\mathbf{v}}[(n+1)\Delta t] = \mathbf{v}(n\Delta t) + \Delta t\mathbf{H}\mathbf{v}(n\Delta t)$$

You can get a second order scheme by averaging the predicted value with the current value as shown in Equation 2-92.

(2-92) $$\mathbf{v}[(n+1)\Delta t] = \mathbf{v}(n\Delta t) + \frac{\Delta t}{2}[\mathbf{H}\mathbf{v}(n\Delta t) + \mathbf{H}\overline{\mathbf{v}}(n\Delta t)]$$

In this case, the x_1, x_2, and x_3 differentials are replaced with suitable central differences, and Equation 2-92 is used as a predictor-corrector scheme of second order.

Splitting

It is possible to rewrite Equation 2-81 as Equation 2-93, where $\mathbf{A}_0$, $\mathbf{B}_0$, and $\mathbf{E}_0$ are given by Equation 2-94 and Equation 2-95, respectively.

(2-93) $$\mathbf{E}\frac{\partial \mathbf{v}}{\partial t} = \mathbf{A}_0\frac{\partial \mathbf{v}}{\partial x} + \mathbf{B}_0\frac{\partial \mathbf{v}}{\partial y}$$

(2-94)
$$\mathbf{A_0} = \begin{bmatrix} 0 & 0 & 1 & 0 & 0 \\ 0 & 0 & 0 & 1 & 0 \\ 1 & 0 & 0 & 0 & 0 \\ 0 & 0 & 0 & 0 & 0 \\ 0 & 1 & 0 & 0 & 0 \end{bmatrix} \quad \mathbf{B_0} = \begin{bmatrix} 0 & 0 & 0 & 0 & 1 \\ 0 & 0 & 0 & 1 & 0 \\ 0 & 0 & 0 & 0 & 0 \\ 0 & 1 & 0 & 0 & 0 \\ 1 & 0 & 0 & 0 & 0 \end{bmatrix}$$

(2-95)
$$\mathbf{E_0} = \begin{bmatrix} \rho & 0 & 0 & 0 & 1 \\ 0 & \rho & 0 & 1 & 0 \\ 0 & 0 & \frac{\lambda+2\mu}{(\lambda+2\mu)^2-\mu^2} & \frac{-\mu}{(\lambda+2\mu)^2-\mu^2} & 0 \\ 0 & 0 & \frac{-\mu}{(\lambda+2\mu)^2-\mu^2} & \frac{\lambda+2\mu}{(\lambda+2\mu)^2-\mu^2} & 0 \\ 0 & 0 & 0 & 0 & \frac{1}{\mu} \end{bmatrix}$$

If we let $\mathbf{V} = \mathbf{E_0 v}$, $\mathbf{F} = \mathbf{A_0 v}$, and $\mathbf{K} = \mathbf{B_0 v}$, then Equation 2-93 takes the form of Equation 2-96.

(2-96)
$$\frac{\partial \mathbf{V}}{\partial t} = \frac{\partial \mathbf{F}}{\partial x} + \frac{\partial \mathbf{K}}{\partial y}$$

Equations of the form in Equation 2-96 are called *divergence free*. These equations are easily *split* into two much simpler equations which are then solved by splitting methods. The simple conceptual idea is to solve the equation in one direction and then the other, followed by reversing the solution order for the next time stamp. Suppose we let L_x represent one finite difference update using only the x variables and L_y represent one finite difference update using only the y variables. The general process for updating then uses the formula in Equation 2-97.

(2-97)
$$\mathbf{V^{n+2}} = L_x L_y L_y L_x \mathbf{V}^n$$

Thus, all we have to do is specify one or the other of the solution schemes L_x, or L_y, and we will have the other, completely by symmetry. A fourth order in space, second order in time predictor-corrector scheme for L_x takes the form of Equation 2-98.

(2-98)
$$\begin{aligned} \overline{\mathbf{V}}_{i,j} &= \mathbf{V}^k_{i,j} + \frac{\Delta t}{\Delta x}\left[(7\mathbf{F}^k_{i+1,j} - \mathbf{F}^k_{i,j}) - (\mathbf{F}^k_{i+2,j} - \mathbf{F}^k_{i+1,j})\right] \\ \mathbf{V}^{k+1}_{i+1,j} &= \frac{1}{2}\left[V^k_{i,j} + \overline{\mathbf{V}}_{i,j} + \frac{\Delta t}{\Delta x}\left\{(7\overline{\mathbf{F}}_{i,j} - \overline{\mathbf{F}}_{i-1,j}) - (\overline{\mathbf{F}}_{i-2,j} - \overline{\mathbf{F}}_{i-1j})\right\}\right] \end{aligned}$$

Propagation Stability

Each of the various finite difference methods you might construct contains a ratio of the form $\frac{v\Delta t}{\Delta v}$, where v is one of the spatial increments Δx, Δy or Δz. It might come as somewhat of a surprise that if this ratio is too large, the propagation scheme it helps define will not be stable. An unstable scheme will eventually produce excessively large numbers and exceed the numerical accuracy of the machine it is running on.

Derivation of a formula that can provide an accurate bound for these ratios requires that we first relate frequency to wavenumber. To do this in a simple manner, we begin with the 1-D version of the Lax-Wendroff discrete pressure equation (Equation 2-17), as shown in Equation 2-99, where v is velocity.

(2-99)
$$\frac{1}{\Delta t^2}\left(p(t+\Delta t) - 2p(t) + p(t-\Delta t) - \sum_{i=2}^{i=\infty} \frac{\partial^{2i} p}{\partial t^{2i}} \frac{\Delta t^{2i}}{2i!}\right) = v^2 \frac{\partial^2 p}{\partial t^2}$$

To make our life a bit easier, we assume a solution of the form $\exp[ik_x x - \omega\Delta t]$ and ignore the higher order terms to obtain the dispersion relation in Equation 2-100 and Equation 2-101.

(2-100)
$$\frac{1}{\Delta t^2}[2\cos(\omega\Delta t) - 2] = \frac{4}{\Delta t^2}\sin^2\left(\frac{\omega\Delta t}{2}\right) = v^2 k_x^2$$

(2-101)
$$\frac{2}{\Delta t}\sin\left(\frac{\omega\Delta t}{2}\right) = v k_x$$

Although the true dispersion relation for the 1-D equation has $c = \frac{\omega}{k_x}$, Equation 2-102 says that the discrete velocity is greater than the true velocity.

(2-102)
$$\bar{v} = \frac{v}{\frac{\sin(\pi f \Delta t)}{\pi f \Delta t}}$$

Thus, to avoid explosive growth, we must have the relation in Equation 2-103.

(2-103)
$$\Delta t \le \frac{2}{\pi}\left(\frac{\Delta x_{min}}{v_{max}}\right)$$

A similar analysis shows that to achieve stable isotropic elastic ($P - SV$) waves, we must have the relation in Equation 2-104.

(2-104)
$$\Delta t \le \frac{\Delta x_{min}}{\sqrt{v_P^2 + v_{SV}^2}}$$

The important aspect of this analysis is that we cannot choose our time step size arbitrarily. We must use the appropriate version of Equation 2-103 or Equation 2-104 to assure ourselves that the calculations we perform and, consequently, the waveform we produce will not grow exponentially.

Model Boundaries

This section describes the things we must do to handle model boundaries, which can consist of either free or non-free surfaces.

Free Surfaces

Handling a free surface is probably the most complex of the various problems that arise in seismic modeling exercises. The literature on this aspect of the synthesis is quite vast and outside the scope of what we wish to discuss here. We leave detailed investigation of this to you, if you are interested.

However, one of the more appealing methods is discussed by Lavendar in his 1988 paper on P-SV modeling, and illustrated in Figure 2-25. The essential difference lies in how each layer is handled. Turning free surface reverberations on (or off) controls whether or not synthetic data contains multiples and ghosts.

Figure 2-25. Free Surface versus Non-Free Surface Layers

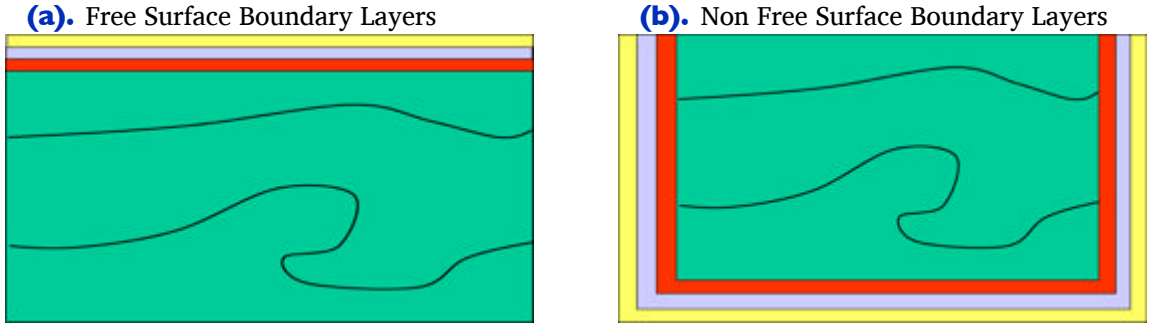

The free surface at the top of the model is padded above with a fictitious set of nodes. Since a free surface implies that no normal or shear stresses are active there, we can set $\tau_{2,2} = 0$ and $\tau_{1,2} = 0$ at the top. The shear stress boundary condition is handled by setting it to zero at $z = 0$ as well. The normal stress is not defined at the top boundary but is forced to zero by making the normal stress antisymmetric for the first two rows above

the free surface, as shown in Equation 2-105.

$$(\tau_{22})_{-1,i} = -(\tau_{22})_{0,i}$$
$$(\tau_{22})_{-2,i} = -(\tau_{22})_{1,i} \quad (2\text{-}105)$$

Non Free Surfaces

There are a variety of approaches for handling the other boundaries in a typical seismic Earth model. The three most popular methods are what are called sponge boundary conditions: Absorbing, boundary conditions, and the so-called perfectly matched layers.

Sponge Boundaries—Absorbing

The idea behind sponge boundary conditions is to modify the propagating equation by adding viscosity to the equation along the boundary. This is normally accomplished by writing Equation 2-106, where γ is an absorbing parameter chosen to produce a wave that decreases in amplitude with distance.

$$\frac{\partial}{\partial t}\begin{bmatrix} p \\ q \end{bmatrix} = \begin{bmatrix} -\gamma & 1 \\ -\rho v^2 \nabla \cdot \frac{1}{\rho}\nabla & -\gamma \end{bmatrix}\begin{bmatrix} p \\ q \end{bmatrix} + \begin{bmatrix} 0 \end{bmatrix} \quad (2\text{-}106)$$

The value of γ is usually chosen to have exponential decay within the defined boundary zone and is zero within the model dimensions. Note that when $\gamma = 0$, the solution to the equation is, in fact, p.

For the finite element method, sponge boundaries can be implemented by changing the definition of $\varphi(U, V)$ to Equation 2-107, where α and β are the damping factors in each of the boundary layers.

$$\varphi(U, V) = (1 + \alpha)\int_{\Omega} \frac{k^2}{\rho} UV d\Omega + (\beta + 1)\int_{\Omega} \frac{1}{\rho}\nabla U \cdot \nabla V d\Omega \quad (2\text{-}107)$$

Sponge Boundaries—Paraxial Boundary Conditions

Paraxial boundaries are based on the one-way wave equation and within the boundary layers take the form in Equation 2-108, where $|\alpha_j| < \frac{\pi}{2}$ for all j (Higdon 1991).

$$\left\{\prod_{j=1}^{j=J}\left[(cos\alpha_j)\frac{\partial}{\partial t} - v\frac{\partial}{\partial x}\right]\right\} p = 0 \quad (2\text{-}108)$$

This equation works because each factor, $\cos(\alpha_j)\frac{\partial p}{\partial t} - v\frac{\partial p}{\partial x}$, is an annihilator of any wave arriving at an angle α_j.

Sponge Boundaries—Perfectly Matched Layers

Perfectly matched layers are a modern treatment of the sponge boundary conditions. In this setting, the spatial derivatives are modified so that we have Equation 2-109.

(2-109)
$$\frac{\partial}{\partial x} \longrightarrow \frac{1}{1 + \frac{i\sigma(x)}{\omega}} \frac{\partial}{\partial x}$$

FEM versus FDM Differences

The finite element method (FEM) and finite difference method (FDM) are alternative ways of approximating solutions of partial differential equations. The differences between FEM and FDM are:

- FDM is an approximation to the differential equation while FEM is an approximation to its solution.
- The most attractive feature of FEM is its ability to handle complicated geometries (and boundaries) with relative ease. While FDM is restricted, in its basic form, to handling rectangular shapes and simple alterations of those shapes, the handling of geometries in FEM is theoretically straightforward.
- The most attractive feature of FDM is that it can be very easy to implement and does not require the inversion of an extremely large matrix.
- In some cases, FEM can be considered to be equivalent to FDM. Choosing basis functions as either piecewise constant functions or Dirac delta functions produce a FDM type method. In both approaches, the approximations are defined on the entire domain, but need not be continuous.
- FEM is generally considered to be more mathematically sound then FDM, and more accurate. Typically, the quality of the approximation between grid points is excellent in FEM but poor in FDM.
- The quality of an FEM approximation is often higher than in the corresponding FDM approach, but this is extremely problem dependent. There are numerous examples to the contrary.

Generally, FEM is the method of choice in all types of structural analysis problems, but it has not proven to be of tremendous value in seismic simulation or migration. The biggest reason for this is the tremendous size of the impedance matrix, **S**, which means it is quite difficult to handle.

Two-Way Implicit Modeling

With the exception of the finite element method, the two-way approaches described earlier are what are usually referred to as *explicit* schemes. They forward march source samples one step at a time. The finite element method is close to an *implicit* approach since finding the solution requires the inversion of a matrix. There are certainly approaches to seismic modeling that can be framed in an implicit sense, but those are equation dependent and will not be discussed further in this book.

One-Way Modeling

Although its not quite mathematically correct, Equation 2-17 is sometimes factored into two first order equations. The factorization leads to two separate first-order equations in z. Equation 2-110 illustrates the nature of the factorization.

$$\left(\frac{\partial}{\partial z}-\sqrt{\frac{1}{v^2}\frac{\partial^2}{\partial t^2}-\frac{\partial}{\partial x}\frac{1}{\rho}\frac{\partial}{\partial x}}\right)\left(\frac{\partial}{\partial z}+\sqrt{\frac{1}{v^2}\frac{\partial^2}{\partial t^2}-\frac{\partial}{\partial x}\frac{1}{\rho}\frac{\partial}{\partial x}}\right)p=0 \tag{2-110}$$

In the case where the density, ρ, is constant, or, even better, equal to 1, the equations simplify further and are what are usually used when applied as part of a migration.

Clearly, the thought process to arrive at this product assumes that the two cross-product terms commute, and thus their difference is zero, but this assumption of commutation is simply not mathematically correct. Nevertheless, is can be shown that suitable approximations to either of the first-order equations that result from the factorization honor the wavefront travel times of the original two-way equation. Because wavefields are no longer allowed to travel in any direction other than upward or downward, the amplitude of the propagation cannot be correct.

In the case of normal full-wave propagation, the impinging wavefield energy creates a new source at the point of impact. Regardless of source wavefield type (that is, compressional or shear), the new source radiates energy in all directions weighted by the reflection strength for upward traveling wave, transmission strength for the downward traveling waves, and angle of the reflecting bed. This is an extremely important concept for all of the discussion that follows. It actually allows us to think in terms of separating wavefields into upward only and downward only propagation directions. Each factor in Equation 2-110 does precisely that. The first factor governs downward only traveling waves while the second permits only upward traveling waves.

Once a suitable approximation for the square root term has been found, almost any of these methods can be applied to synthesize data of the type required by the equation. That is, when the downward factor is used, you can propagate wavefields downward but not upward; when the upward factor is used, you can propagate wavefields upward but not downward. Thus, these equations greatly limit the extent to which full wavefield seismic can be generated.

One Way Implicit Finite Difference Methods

There are many known approximations for the square root in Equation 2-110. Each such approximation has its own pros and cons, and each has its own unique limit to the downward propagation angle it will tolerate. One of the better known square-root approximations is Equation 2-111.

$$\sqrt{1 - X^2} = 1 - \frac{4 - 3X^2}{4 - X^2} \tag{2-111}$$

If we apply this approximation to the square root in Equation 2-110, we obtain Equation 2-112.

$$\sqrt{\frac{1}{v^2}\frac{\partial^2}{\partial t^2} - \frac{\partial}{\partial x}\frac{1}{\rho}\frac{\partial}{\partial x}} \approx \frac{1}{v}\frac{\partial}{\partial t} - \frac{\frac{4}{v^2}\frac{\partial^2}{\partial t^2} - 3\frac{\partial}{\partial x}\frac{1}{\rho}\frac{\partial}{\partial x}}{\frac{4}{v^2}\frac{\partial^2}{\partial t^2} - \frac{\partial}{\partial x}\frac{1}{\rho}\frac{\partial}{\partial x}} \tag{2-112}$$

Equation 2-112 leads directly to a downward propagation equation of the rather complex form in Equation 2-113.

$$\frac{\partial p}{\partial z} = \frac{1}{v}\frac{\partial p}{\partial t} - \frac{\frac{4}{v^2}\frac{\partial^2 p}{\partial t^2} - 3\frac{\partial p}{\partial x}\frac{1}{\rho}\frac{\partial p}{\partial x}}{\frac{4}{v^2}\frac{\partial^2}{\partial t^2} - \frac{\partial}{\partial x}\frac{1}{\rho}\frac{\partial}{\partial x}} \tag{2-113}$$

At first glance, this equation may seem to be somewhat intractable for any finite difference approach. The trick to putting this into a more useable form is to clear fractions to obtain Equation 2-114.

$$\left(\frac{4}{v^2}\frac{\partial^2 p}{\partial t^2} - \frac{\partial p}{\partial x}\frac{1}{\rho}\frac{\partial p}{\partial x}\right)\frac{\partial p}{\partial z} = \left(\frac{4}{v^2}\frac{\partial^2 p}{\partial t^2} - \frac{\partial p}{\partial x}\frac{1}{\rho}\frac{\partial p}{\partial x}\right)\frac{1}{v}\frac{\partial p}{\partial t} + 3\frac{\partial p}{\partial x}\frac{1}{\rho}\frac{\partial p}{\partial x} - \frac{4}{v^2}\frac{\partial^2 p}{\partial t^2} \tag{2-114}$$

Equation 2-114 in 3D becomes Equation 2-115.

$$\begin{aligned}\left(\frac{4}{v^2}\frac{\partial^2 p}{\partial t^2} - \frac{\partial p}{\partial x}\frac{1}{\rho}\frac{\partial p}{\partial x} - \frac{\partial p}{\partial y}\frac{1}{\rho}\frac{\partial p}{\partial y}\right)\frac{\partial p}{\partial z} \;=\; &\left(\frac{4}{v^2}\frac{\partial^2 p}{\partial t^2} - \frac{\partial p}{\partial x}\frac{1}{\rho}\frac{\partial p}{\partial x} - \frac{\partial p}{\partial y}\frac{1}{\rho}\frac{\partial p}{\partial y}\right)\frac{1}{v}\frac{\partial p}{\partial t} \\ &+ 3\left(\frac{\partial p}{\partial x}\frac{1}{\rho}\frac{\partial p}{\partial x} + \frac{\partial p}{\partial y}\frac{1}{\rho}\frac{\partial p}{\partial y}\right) - \frac{4}{v^2}\frac{\partial^2 p}{\partial t^2}\end{aligned} \tag{2-115}$$

If we then approximate the derivatives via some form of the finite difference stencils discussed in previous sections, we can rearrange the problem, converting Equation 2-113 into a matrix style system of the form in Equation 2-116.

$$\mathbf{A}p(z + \Delta z) = \mathbf{B}p(z) \tag{2-116}$$

Solving this system amounts to inverting **A**. The need to employ finite-differences in time can make this a very complicated task in 3D. Consequently, this XT method has not enjoyed a lot of popularity in either forward modeling or imaging for 3D projects.

Fourier-Based Methods

This section discusses the several Fourier-based methods for solving modeling and imaging projects.

FX Finite Difference Methods

The factorization in Equation 2-110 can also be done in the Fourier or frequency domain by simply rewriting it in the form of Equation 2-117.

(2-117) $$\left(\frac{\partial}{\partial z} - i\sqrt{\frac{\omega^2}{v^2} + \frac{\partial}{\partial x}\frac{1}{\rho}\frac{\partial}{\partial x}}\right)\left(\frac{\partial}{\partial z} + i\sqrt{\frac{\omega^2}{v^2} + \frac{\partial}{\partial x}\frac{1}{\rho}\frac{\partial}{\partial x}}\right)p = 0.$$

In this case, Equation 2-114 becomes Equation 2-118.

(2-118) $$\left(\frac{4\omega^2}{v^2}p + \frac{\partial p}{\partial x}\frac{1}{\rho}\frac{\partial p}{\partial x}\right)\frac{\partial p}{\partial z} = \left(\frac{4\omega^2}{v^2}p + \frac{\partial p}{\partial x}\frac{1}{\rho}\frac{\partial p}{\partial x}\right)\frac{i\omega}{v}p - 3\frac{\partial p}{\partial x}\frac{1}{\rho}\frac{\partial p}{\partial x} - \frac{4\omega^2 p}{v^2}$$

In 3D, Equation 2-118 becomes Equation 2-119.

(2-119) $$\left(\frac{4\omega^2}{v^2}p + \frac{\partial p}{\partial x}\frac{1}{\rho}\frac{\partial p}{\partial x} + \frac{\partial p}{\partial y}\frac{1}{\rho}\frac{\partial p}{\partial y}\right)\frac{\partial p}{\partial z} = \left(\frac{4\omega^2}{v^2}p + \frac{\partial p}{\partial x}\frac{1}{\rho}\frac{\partial p}{\partial x} + \frac{\partial p}{\partial y}\frac{1}{\rho}\frac{\partial p}{\partial y}\right)\frac{i\omega}{v}p - \left(3\frac{\partial p}{\partial x}\frac{1}{\rho}\frac{\partial p}{\partial x} + \frac{\partial p}{\partial y}\frac{1}{\rho}\frac{\partial p}{\partial y}\right) - \frac{4\omega^2 p}{v^2}$$

Equation 2-119 has the generalized form in Equation 2-120.

(2-120) $$\mathbf{A}(\omega)p(z + \Delta z) = \mathbf{B}(\omega)p(z)$$

Once again, inversion of $\mathbf{A}(\omega)$ is a necessity. In the frequency domain, this matrix is normally diagonally dominant and usually relatively easy to compute. Note that we are

solving this as an equation in z for each ω. We are in effect computing $p(z + \Delta z)$ from $p(z)$ so that the $\mathbf{A}(\omega)$ matrix has two dimensions and not three. This further simplifies the issue and makes this method one of the more tractable one way implicit methodologies. Nevertheless, the process is not straightforward and usually requires a splitting approach to make it efficient.

One clear advantage of this approach to one-way forward modeling is the elimination of finite difference approximations in time. In the frequency domain, the partial differentials are simple complex multiplications. Since they are applied across the entire frequency band, the temporal derivatives are as precise as they can be.

Pseudo-Spectral Methods

Pseudo-spectral methods are based on the utilization of Fourier transforms in the calculation of spatial derivatives (see D. Kosloff and E. Baysal). Again, using the 2D version of Equation 2-17 as the base, we first apply a central difference scheme in the time direction and then use Fourier transforms to calculate all spatial derivatives. As an example, consider the discrete formulation in Equation 2-121, where L represents the discrete operator containing the spatial derivatives in both x and z.

(2-121) $$p_{i,j}^{k+1} = 2p_{i,j}^{k} - p_{i,j}^{k-1} - v^2 \Delta t^2 L p_{i,j}^{k} + s_{i,j}^{k}$$

To calculate the discrete version of the term $\frac{\partial p}{\partial x}\frac{1}{\rho}\frac{\partial p}{\partial x}$, we first Fourier transform in the x-direction on p, multiply by the discrete-spatial wave-number ik_x, and then inverse Fourier transform to get $\frac{\partial p}{\partial x}$.

This is followed by a repeat of a Fourier-multiply-Fourier inverse step to get $\frac{\partial p}{\partial x}\frac{1}{\rho}\frac{\partial p}{\partial x}$.

When the process has been completed along all x-lines, a similar calculation is performed to get $\frac{\partial p}{\partial z}\frac{1}{\rho}\frac{\partial p}{\partial z}$.

Working in 3D is just as simple and requires only that we perform one more transform sequence in the y direction.

The great advantage of this process is accuracy. Using the Fourier transform for the spatial derivatives is identical to applying a central difference with the number of coefficients equal to the half length of the discrete transform.

Once we understand that the Fourier transformation converts differentials, $\frac{\partial u}{\partial x}$, into frequency domain multiplications of the form $ik_x u(x)$, it is quite natural to want to Fourier transform Equation 2-17 over all variables and convert the resulting PDE into a simple algebraic equation. Unfortunately, because the velocity, $v(x, y, z)$, and the

density, $\rho(x,y,z)$, are both potentially functions of three independent variables, Fourier transformation would result in a frequency domain convolution, which is not a much simpler algebraic equation.

Constant Velocity FK Modeling

When the velocity, v, is constant, Fourier transformation over all the variables produces Equation 2-122 everywhere except at the source.

(2-122) $$(k_z^2 + k_z^2 - \frac{\omega^2}{v^2})\, u(k_z, k_x, \omega) = 0$$

Thus, for k_z and $u(k_z, k_x, \omega)$, we get Equation 2-123 and Equation 2-124, respectively.

(2-123) $$k_z = \pm\sqrt{\frac{\omega^2}{v^2} - k_x^2}$$

(2-124) $$u(k_z, k_x, \omega) = u\left(\sqrt{\frac{\omega^2}{v^2} - k_x^2}, k_x, \omega\right)$$

The key point is that we only need to know $p(z = 0, x, t)$ to determine k_z through a Fourier transform over x and t.

Thus, to do modeling, we simply define $p(0, x_0, t) = s(x_0, t)$, set $p(0, x, t) = 0$ elsewhere, Fourier transform over x and t, define $p(k_z, k_x, \omega)$ through Equation 2-123, and then inverse transform to get our one-way modeled data $p(z, x, t)$. Whether this represents upward or downward traveling waves is purely dependent on the choice of sign in Equation 2-123.

Since this method is almost totally dependent on extremely efficient Fourier transforms, you would think that modeling using this method would be very popular. Unfortunately, the equations in this section are valid only when the velocity is constant. As we will see, overcoming this limitation has produced many of the modern one-way algorithms for imaging, but has not resulted in a satisfactory formalism for detailed high resolution modeling. Methods in this section can progress wavefields in one direction or the other, but unlike the two-way methods, they do not automatically generate waves traveling in every possible direction.

Phase-Shift Modeling

When the velocity, $v = v(z)$, is just a function of z alone, and the density, ρ, is constant, we can Fourier transform over t, x to get Equation 2-125.

(2-125) $$\frac{\partial^2 p}{\partial z^2} = \left[-\frac{\omega^2}{v^2(z)} + k_x^2\right] p$$

If we now factor Equation 2-125 and choose the downward propagating equation as the one of interest, we can write Equation 2-126.

(2-126) $$\frac{\partial p}{\partial z} = -\left[\sqrt{\frac{\omega^2}{v^2(z)} - k_x^2}\right] p$$

If we think of this equation as a first order ordinary differential equation in z, we can immediately write its solution in the form of Equation 2-127, where k_z has the value in Equation 2-128.

(2-127) $$p(k_x, z + \Delta z, \omega) = \exp[ik_z \Delta z]\ p(k_x, z, \omega)$$

(2-128) $$k_z = \sqrt{\frac{\omega^2}{v^2(z)} - k_x^2}$$

Note that the exponential term in Equation 2-127 represents a pure phase shift for each frequency ω. The process is visualized quite naturally in Figure 2-26. Starting at the top for downward propagation and at the bottom for upward propagation, the one-way phase shift method simply shifts the wavefield from one layer to the next in a simple and straightforward manner. To start the modeling process, you initialize the wavefield $p(z = 0, x_0, t) = s(x_0, t)$ at $z = 0$ with a suitable source, Fourier transform over time and begin downward propagation using Equation 2-127

Figure 2-26. FK domain depth-slice by depth-slice continuation for $v(z)$ velocity models. This is called phase shift modeling.

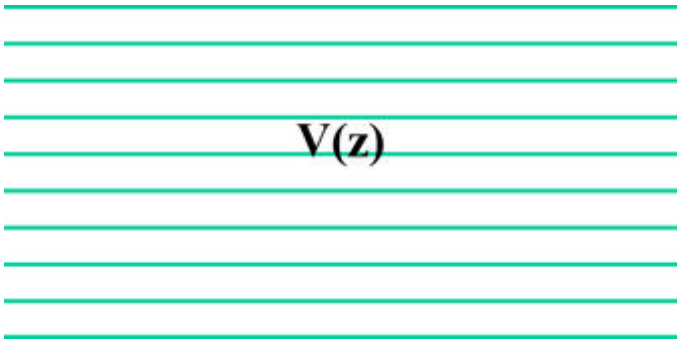

While we recognize that the accuracy of the phase-shift method is highly dependent on the number of terms we use to approximate the series for the exponential, the ultimate accuracy is dependent only on the current computer language approximations for the exponential and the square root. The ultimate limitation of this method, like the pure FK method discussed previously, is the restriction that the velocity vary only in the vertical direction. The frequency slice process specified by Equation 2-127 has an immediate and more or less obvious extension to 3D.

Phase Shift Plus Interpolation (PSPI) Modeling

When the sound speed, $v(x,z)$, varies laterally as well as vertically, the wavefield shifts are no longer uniform. One approach to handling this problem is to first perform a number, n, of pure phase shifts using a uniform set of of velocities lying between the minimum and maximum values of $v(x,z)$. Interpolation of the appropriate wavefields at any given x along the common depth slice at z approximates the wavefield corresponding to the true velocity $v(x,z)$ at x. Figure 2-27 illustrates the concept.

Figure 2-27. PSPI FK domain depth-slice by depth-slice continuation for $v(x,z)$ velocity models.

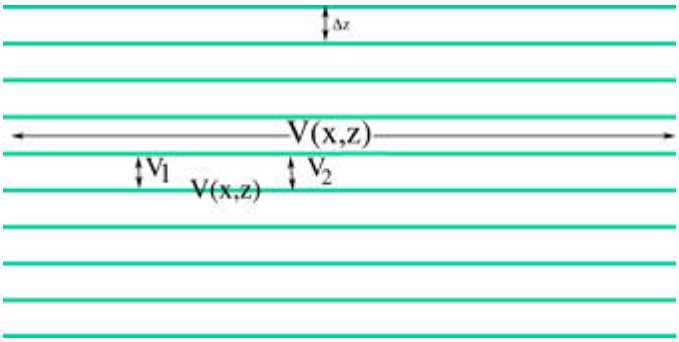

The problem with this approach revolves around the complexities of performing the interpolation. Key questions arise as to whether interpolation in space-time or frequency-space is the more optimum method. Because of the difficulties associated with the need for interpolation, PSPI continuations frequently have difficulty imaging steeply dipping events. As a result, considerable research focused on finding a better approach.

Dual Domain or FKX One-Way Methods

Because of the incredible efficiency of the Fast Fourier transform, it did not take long for several authors to investigate the possibility of avoiding the need for wavefield interpolation by using approximations that split the computations between the FK and FX domains. This required multiple transforms for each up or down shift, but because of the efficiency of the Fourier transform, this was considered worth the extra effort. The idea underlying this form of the process is again a Taylor series approximation. If the velocity, $v(x,z)$ varies laterally, the first-term Taylor series expansion of the k_z term in Equation 2-128 around some fixed reference velocity, $v_{ref} = v_{ref}(z)$, has the form of Equation 2-129, where $s_{ref} = \frac{1}{v_{ref}}$ is the reference slowness and $k_z^{ref} = \sqrt{s_{ref}^2\omega^2 - k_x^2}$.

(2-129)
$$k_z = k_z^{ref} + \frac{dk_z}{ds_{ref}}\Delta s$$

In this case,

(2-130) $$\frac{dk_z}{ds_{ref}} = \frac{\omega}{\sqrt{s_{ref}^2\omega^2 - k_x^2}}$$

Using the approximation in Equation 2-111, a little algebraic manipulation yields Equation 2-131, so that Equation 2-132, where $k_{ref}^2 = \frac{\omega^2}{v_{ref}^2}$.

(2-131) $$\frac{dk_z}{ds_{ref}} = \omega\left[1 + \frac{2k_x^2}{4k_{ref}^2 - 3k_x^2}\right]$$

(2-132) $$k_z \approx \sqrt{k_{ref}^2 - k_x^2} + \omega\Delta s + \omega\Delta s\frac{2k_x^2}{4k_{ref}^2 - 3k_x^2}$$

You could, of course, use additional terms of the Taylor series to try to increase the accuracy of the approximation, but, as we will see, the third term in Equation 2-132 can be quite difficult to implement.

Split-Step Methods

Paul Stoffa at the University of Texas in Austin was one of the first to utilize Equation 2-132. He and his colleagues in Austin and at Delft University in Holland simply truncated the series for k_z to Equation 2-133, and then noted that the first term was just a phase shift in the FK domain while the second is a similar phase-shift in the FX domain.

(2-133) $$k_z \approx \sqrt{k_{ref}^2 - k_x^2} + \omega\left[\frac{1}{v} - \frac{1}{v_{ref}}\right]$$

Summing over all frequencies produces the image at the current Δz. Fourier transforming back to the FK domain begins the process for the next $z + \Delta z$. Although this method proves to be somewhat inaccurate when compared to good implementations of PSPI, it is significant in that it requires no interpolation at all. It provides a direct correction in the FX domain after an initial phase shift.

Extended Split Step Methods

The extended phase screen method is probably more accurately referred to as split-step plus interpolation or $SSPI$. It attempts to increase the overall accuracy of the preceding process by using multiple reference velocities in exactly the same manner as $PSPI$.

Higher Order FKX Methods

Higher order methods based on Equation 2-132 must find ways to handle the third term, Equation 2-134.

(2-134) $$k_z^{fd} = \omega \Delta s \frac{2k_x^2}{4k_{ref}^2 - 3k_x^2}$$

While it might appear that this term can be handled directly by some form of transform between the FK and KX or maybe FX domains, the denominator implies the existence of a singularity and therefore a potentially difficult instability. Two approaches have evolved in an attempt to handle the instability. One is the phase-screen or pseudo-phase screen method of Ru Shan Wu at the University of California at Santa Cruz and the other is the Fourier Finite Difference (FFD) method of D. Ristow and T. Rühl. In fact, both of these methods use what is called an implicit finite difference technique to implement the term stably.

Note that from an implementation point of view, what we do in practice is first form Equation 2-135, inverse Fourier transform over k_x and form Equation 2-136, and finally try to compute Equation 2-137 in some domain or the other.

(2-135) $$p_1(k_x, z + \Delta z, \omega) = \exp\left(ik_z^{ref} \Delta z\right) p(k_x, z, \omega)$$

(2-136) $$p_2(x, z + \Delta z, \omega) = \exp\left(i\omega \Delta s \Delta z\right)$$

(2-137) $$p(x, z + \Delta z, t) = \exp\left(ik_z^{fd} \Delta z\right) p_2(k_x, z, \omega)$$

It should be clear that because the third term contains both spatial and wavenumber terms, this calculation might not be straightforward. The actual trick is to approximate the exponential one more time in the form of Equation 2-138, substitute into Equation 2-137, and clear fractions to get Equation 2-139.

(2-138) $$\exp\left(ik_z^{fd} \Delta z\right) = \frac{1 + i\omega \Delta s \frac{2k_x^2}{4k_{ref}^2 - 3k_x^2} \frac{\Delta z}{2}}{1 - i\omega \Delta s \frac{2k_x^2}{4k_{ref}^2 - 3k_x^2} \frac{\Delta z}{2}}$$

(2-139) $$\left(4k_{ref}^2 - 3k_x^2 - i\omega \Delta s 2k_x^2 \Delta z\right) p(k_x, z + \Delta z, \omega) = \left(4k_{ref}^2 - 3k_x^2 + i\omega \Delta s 2k_x^2 \Delta z\right) p_2(k_x, z, \omega)$$

If we now inverse transform back to the FX domain, we see that each k_x^2 term becomes a second order partial derivative with respect to x. When these are replaced by central difference approximations, we arrive at a matrix equation of the form in Equation 2-140, so that Equation 2-141.

(2-140) $$\mathbf{Ap} = \mathbf{Bp}_2$$

(2-141) $$\mathbf{p} = \mathbf{A}^{-1}\mathbf{Bp}_2$$

What is nice about this method is that the matrix **A** is usually sparse with a limited number of terms along the diagonal, so in 2D, as described here, inverting the matrix is relatively fast. Moreover, the result is easily stabilized.

However, in 3D, the equivalent **A** matrix is huge and is quite difficult to invert. The problem is usually solved by a splitting technique similar to that in previous sections. Essentially, Equation 2-139 is solved in the x-direction, and then the similar y-direction formula is used to provide a solution in that direction. These methods are alternated as the process proceeds depth-slice by depth-slice until all data is propagated to the appropriate depth.

Figure 2-28 is a simple graphic of how one-way propagators work. Figure 2-28(a) provides the schema for synthesizing purely downward traveling waves, and part (b) is the corresponding propagator for purely upward traveling waves. While these kinds of propagators limit the type of wave that can be propagated, their significance lies mostly in the fact that they are much more computationally efficient then the full two-way versions shown in previous figures. One-way computations can be performed on a depth-slice by depth-slice basis so there is no need to fill in the value at every previous node before continuing. Moreover, extremely efficient Fourier domain methods can be used to reduce computational complexity even further. As a result, one-way methods have enjoyed great popularity and have been the subject of considerable research.

Figure 2-28. A one-way propagator. The black dots have been removed from the propagating stencil. Graphic (a) calculates only downward traveling waves while (b) only permits upward traveling waves.

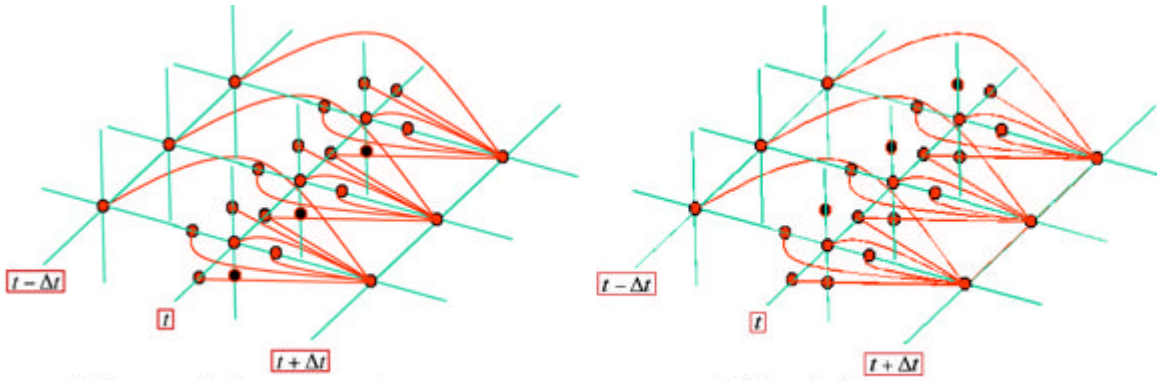

(a) Downward only wave propagator (b) Upward only wave propagator

A Word About Sources

This section describes the sources used to generate the sound waves that are at the center of the seismic migration and modeling process.

Compressional and Shear Point Sources

So far the discussion has been focused on compressional, wave-point sources. Theoretically, such sources radiate energy uniformly in all directions. Mainly because they are easy to generate, point-sources represent the norm in modern seismic data synthesis and acquisition. In media that support shear wave propagation, pure compressional sources also generate shear waves uniformly in all directions. In contrast, real shear wave sources are not so easy to generate, and are impossible to generate in any liquid. Over any media that supports their propagation, shear waves are frequently generated using some kind of scratcher or angled compressional source. In the first case, the scratcher is actually generating a physical source that is fundamentally angled downward, while in the second case the angled compressional source generates most of its energy close to the angle of the compression gun. In either case, the resulting converted-shear wave is frequently too weak to generate sufficient energy for practical use.

Plane Wave Sources

Plane wave sources are all but impossible to generate in the field. However, any reasonable set of shot profiles, $u(x_s, x_r, t)$, from either real data or synthetic data, can be transformed to simulate a plane wave source at some fixed position, x_{s_0}, by simply performing a slant stack over the sources surrounding this central point. The mathematical formula for this in 2D is given by Equation 2-142.

(2-142) $$U(p_s, x_{s_0}, x_r, \tau) = \int u(x_s, x_r, \tau - p \cdot (x_s - x_{s_0}))\, dx_s$$

This formula has a natural extension to 3D, so plane wave shots can be generated for linear moveout in each coordinate direction.

Figure 2-29 describes graphically how a plane wave source is generated from a set of shot profiles. Each source in the set is delayed (or advanced) in time by an amount determined by the desired plane wave moveout and its distance from the central source. The delayed shots are then summed to produced the desired plane wave response. This process is repeated for each required plane wave.

Figure 2-29. Generating a plane wave source by delaying shots.

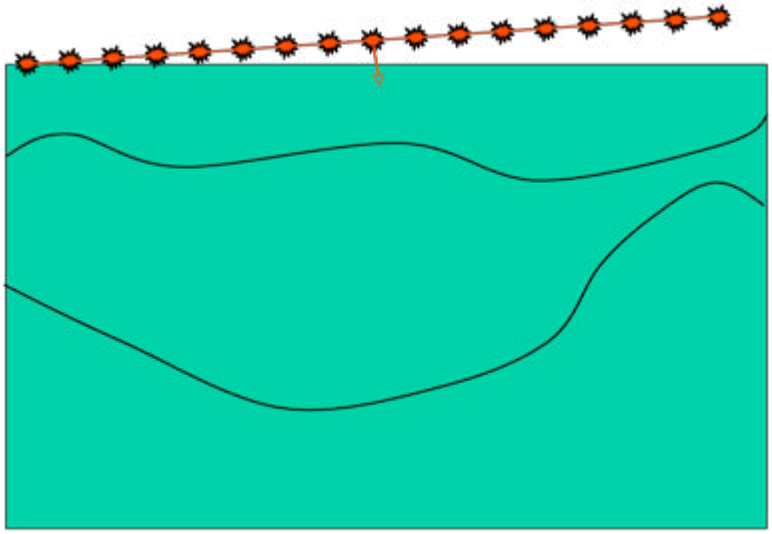

Plane wave sources produce a wavefield with a particular *takeoff* angle. Normally, takeoff angles are measured in degrees from level with zero representing a plane wave in the vertical direction. In the sense that only one plane wave can be generated with this take off angle, the resulting track is unique and the full plane wave is completely determined by this takeoff angle. Figure 2-30 conceptualizes the basic idea in ray theoretic terms. Here we see a plane wave with an apparent takeoff angle of approximately 30 degrees traveling through the subsurface media, as indicated by the ray, and striking a steeply dipping reflection event. The angle of the plane wave at this point also uniquely determines the raypath back to the source so either angle contains sufficient information to completely determine the raypath.

Figure 2-30. A plane wave source and ray.

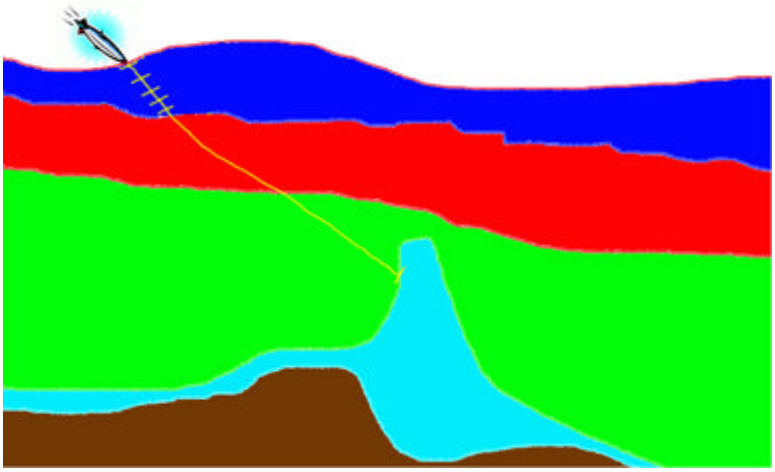

Figure 2-31 illustrates a plane wave propagating through the Marmousi2 model. Figure 2-32 is the actual response of the plane wave in Figure 2-31. While not something the typical geophysicist is familiar with this plane wave shot response can be migrated and imaged just like any traditional point source response.

Figure 2-31. Plane wave sources in the Marmousi2 isotropic elastic model.

(a). Plane Waves at 688 ms **(b).** Plane Waves at 1360 ms

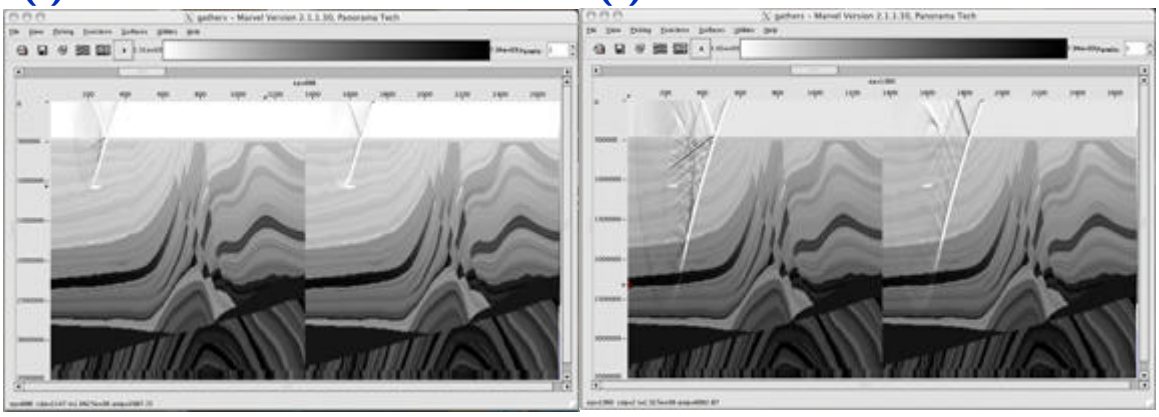

Figure 2-32. Plane wave response over the Marmousi2 model.

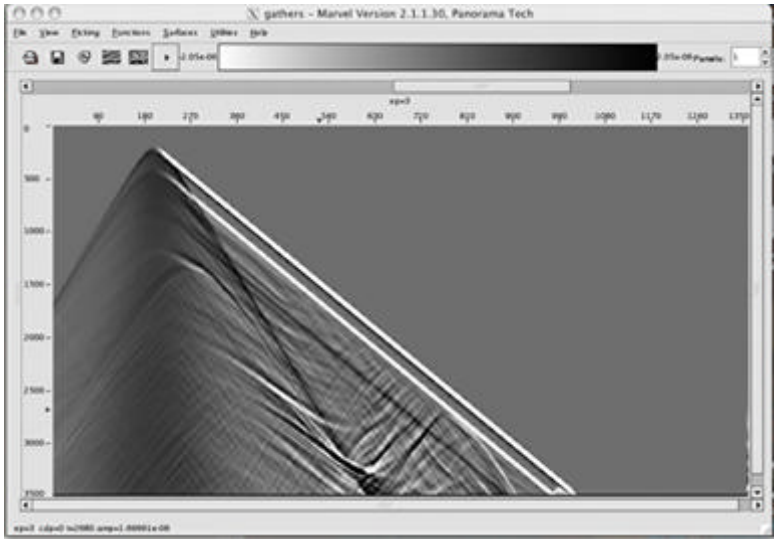

Huygen's Principle and Integral Methods

One of the most powerful seismic modeling concepts, known today as simply the *Huygens Principle*, was expressed some 350 years ago by both Christiaan Huygens and Augustin-Jean Fresnel (Wikipedia contributors, "Huygens–Fresnel principle", Wikipedia, The Free Encyclopedia, Wikipedia link):

> The Huygens–Fresnel principle (named for Dutch physicist Christiaan Huygens, and French physicist Augustin-Jean Fresnel) is a method of analysis applied to problems of wave propagation (both in the far field limit and in near field diffraction). It recognizes that each point of an advancing wave front is in fact the center of a fresh disturbance and the source of a new train of waves; and that the advancing wave as a whole may be regarded as the sum of all the secondary waves arising from points in the medium already traversed. This view of wave propagation helps better understand a variety of wave phenomena, such as diffraction.
>
> For example, if two rooms are connected by an open doorway and a sound is produced in a remote corner of one of them, a person in the other room will hear the sound as if it originated at the doorway. As far as the second room is concerned, the vibrating air in the doorway is the source of the sound. The same is true of light passing the edge of an obstacle, but this is not as easily observed because of the short wavelength of visible light.
>
> Huygens principle follows formally from the fundamental postulate of quantum electrodynamics that wavefunctions of every object propagate over any and all allowed (unobstructed) paths from the source to the given point. It is then the result of interference (addition) of all path integrals that defines the amplitude and phase of the WAVEFUNCTION of the object at this given point, and thus defines the probability of finding the object (say, a photon) at this point. Not only light quanta (photons), but electrons, neutrons, protons, atoms, molecules, and all other objects obey this simple principle.

While we frequently drop his name and simply call this Huygens principle, Fresnel's contribution cannot be minimized, but the part we really need to understand is visualized in Figure 2-33. This principle is usually explained conceptually by saying that the way Huygens arrived at it was based on observations of what happened when he dropped a finite number of balls, N, into the Zuider Zee. When the balls were arranged in a line, what he saw was not N independent events, but something like to a moving line. He saw an envelope of the wavefields rather than the independent wavefield of each separate ball. That being said, it is much more important to think in terms of the formal discussion above. Perhaps a better example of the Huygens–Fresnel principle would be to recognize that a discussion in an adjacent room would actually appear to come from the connecting door. Clearly, the door is acting as a new source and the listener only hears the sound coming from that source.

Figure 2-33(a) shows this for two-way waves and emphasizes that fact we need not think of a single reflector. Parts (b) and (c) of this figure show what happens when waves are allowed to travel in only one direction.

Figure 2-33. A simple graphical interpretation of the Huygens–Fresnel Principle.

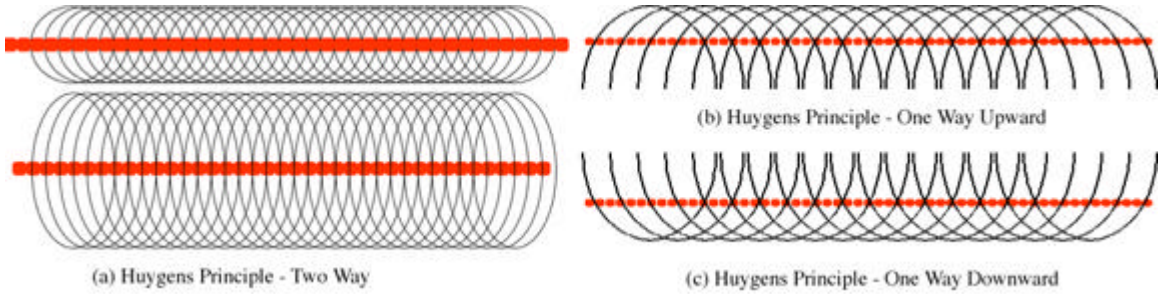

We see that the wavefield due to a reflector, the red flat line in parts (a), (b), and (c), can be thought of as the envelope of an infinite series of point sources. Each point source can be thought of as having been ignited by an impinging wavefront which in part (a) results in both a reflection and a transmission. Parts (b) and (c) visualize what happens when propagation is only allowed upward (b) or downward (c).

The Mathematics of Huygens' Principle

One of the more mathematically complex ways to use this principle is to recognize that regardless of the type of media (that is, acoustic, elastic, or anisotropic), we can think of the total response of any give source in terms of what happens at any given point in the actual model. For example, a source on the surface eventually arrives at some point (x, y, z) with reflectivity $R(x, y, z)$. According to Huygens' principle, the energy of the source then generates a virtual source at (x, y, z), the energy from which then propagates through the entire model, and then perhaps to receivers on the recording surface. In a nutshell, what this really means is that we need only know the response of each point in our model to completely reconstruct the entire wavefield $u(x, y, z, t)$. For the pressure formulation, this concept is mathematically expressed in terms of the so-called Greens' function $G(\vec{x}, \vec{x}_s, t)$ as shown in Equation 2-143, where $\vec{x} = (x, y, z)$ is a generic point in the medium and $\vec{x}_s$ is the vector location of the source.

(2-143)
$$\frac{\partial^2 G}{\partial t^2} - \rho v^2 \nabla \cdot \frac{1}{\rho} \nabla G = \delta(\vec{x} - \vec{x}_s)$$

For a given source, $s(\vec{x}_0, t)$, integration by parts allows us to express the solution p of Equation 2-17 in the integral form of Equation 2-144.

(2-144)
$$p(\vec{x}, t) = \int_{\Omega} G(\vec{x}, \vec{x}_s, t)\, s(\vec{x}_0, t)\, dx_s\, dt$$

This means that the solution to the equation is just the sum of all the point responses of the medium under consideration.

For example, when the velocity and density are constant, the Green's function takes the form in Equation 2-145 and Equation 2-146.

(2-145) $$G(\vec{x},\vec{x}_s,t)=\frac{\delta(t-\frac{|\vec{x}-\vec{x}_s|}{v})}{4\pi|\vec{x}-\vec{x}_s|}$$

(2-146) $$p(\vec{x},t)=\int_\Omega \frac{s(\vec{x}_0,t-\frac{|\vec{x}-\vec{x}_s|}{v})}{4\pi|\vec{x}-\vec{x}_s|}$$

Thus, $p(\vec{x},t)$ is the superposition of all the point responses in the medium due to a source at the point $\vec{x}_0=(x_0,y_0,z_0)$. Another way to say this is that the Green's function, G, is the inverse of the operator in Equation 2-147.

(2-147) $$G=\left(\frac{\partial^2}{\partial t^2}-\rho v^2\nabla\cdot\frac{1}{\rho}\nabla\right)^{-1}$$

Seismic Scattering

In integral form, these formulas lead to what has become known as *domain-integral methods* for solving seismic scattering problems. Although they are important because they divide the seismic propagation scheme into incident and scattered parts, these methods have not been popular for seismic modeling so they are of only a little interest to us.

In theory, the ideas can be based on any of the equations above, but for illustrative purposes, we only consider the pressure case when the density is constant. The basic idea is to assume that the velocity, v, can be expressed as the slowness difference $\frac{1}{v}=\frac{1}{c}-\frac{1}{c_0}$, where c_0 is constant. We can then write Equation 2-148, so that our solution takes the form of Equation 2-149, where p^{inc} is defined by Equation 2-150.

(2-148) $$\left(\nabla\cdot\nabla-\frac{1}{c_0}\frac{\partial^2}{\partial t^2}\right)p=s(\vec{x}_s,t)-\left(\frac{1}{c_0}-\frac{1}{c}\right)\frac{\partial^2 p}{\partial t^2}$$

(2-149) $$p(\vec{x},t)=p^{inc}+\int_\Omega\left(\frac{1}{c_0}-\frac{1}{c}\right)\frac{\partial^2 p}{\partial t^2}$$

(2-150) $$p^{inc} = \int_{\Omega} \frac{s(\vec{x_0}, t - |\vec{x} - \vec{x}_s|/v)}{4\pi|\vec{x} - \vec{x}_s|}$$

Although a bit of a stretch, Figure 2-34 illustrates Huygens' principle in considerable detail. Here we see the wave reflections and transmissions at each point in a given medium.

Figure 2-34. Wave directions and exploding reflectors.

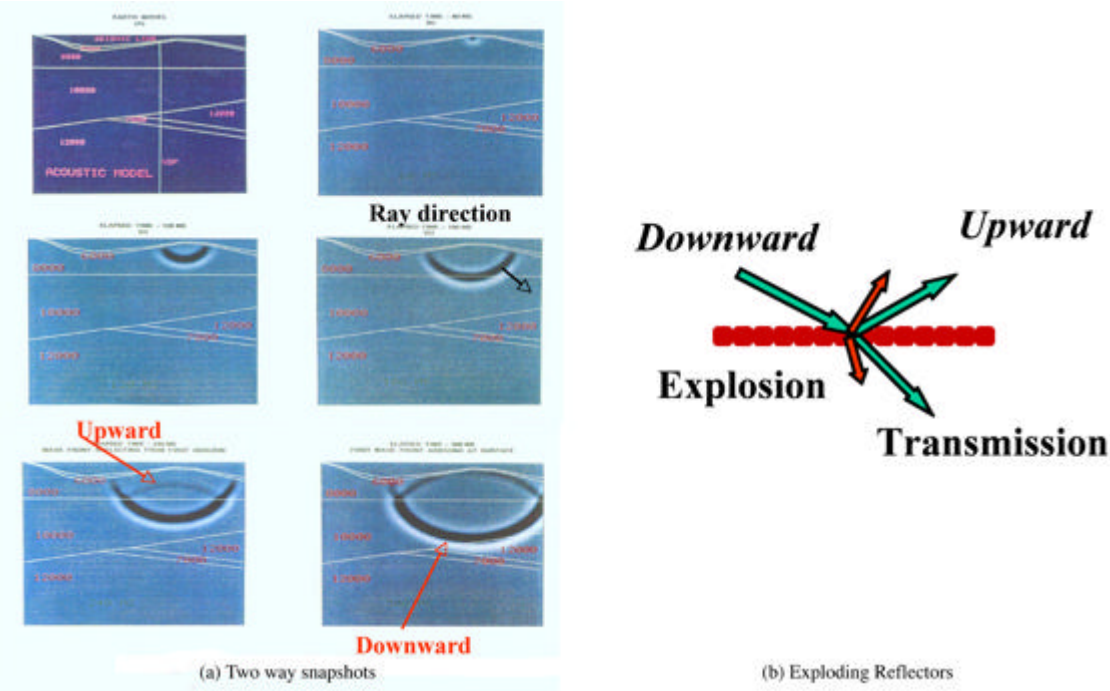

Raytracing

For a source at x_s and receiver at x_r, if we denote the traveltime or *phase* from x_s to x_r by $\varphi(x_r, x_s)$ and the amplitude decay by $A(x_r, x_s)$, we can then write Equation 2-151 in space-time and Equation 2-152 in frequency.

(2-151) $$G(x_r, x_s, t) \approx A(x_r, x_s)\delta(t - \varphi(x_r, x_s)$$

(2-152) $$G(x_r, x_s, \omega) \approx A(x_r, x_s)e^{i\omega\varphi(x_r, x_s)}$$

Substituting into the wave equation in Equation 2-153, we get Equation 2-154.

(2-153) $$\left(\nabla \cdot \nabla - \frac{i\omega^2}{v^2}\right) G(x_r, x_s, \omega) = 0$$

(2-154) $$\left\{ i\omega^2 \left[\left(\nabla\varphi\right)^2 - \frac{1}{v^2(\mathbf{x})} \right] + i\omega\left(2\nabla A \cdot \nabla\varphi + A\Delta\varphi\right)\Delta A \right\} e^{i\omega\varphi} = 0$$

Equating coefficients of powers of $i\omega$ to zero yields the Eikonal equation, Equation 2-155, and the transport equation, Equation 2-156.

(2-155) $$\left(\nabla\varphi\right)^2 - \frac{1}{v^2(\mathbf{x})} = 0$$

(2-156) $$2\nabla A \cdot \nabla\varphi + A\Delta\varphi = 0$$

Simultaneous solution of Equation 2-155 and Equation 2-156 provides the traveltimes and amplitudes necessary to approximate the Green's function in an efficient manner.

While not straightforward, the Eikonal equation, as given here, can be solved by finite differences and/or the method of characteristics. It is called the method of characteristics because it solves the Eikonal equation along rays by simultaneously solving Equation 2-157 and Equation 2-158. The method of characteristics is usually referred to more traditionally as raytracing.

(2-157) $$\frac{d\mathbf{x}}{d\sigma} = \mathbf{p}$$

(2-158) $$\frac{d\mathbf{p}}{d\sigma} = \nabla\left[\frac{1}{2v(\mathbf{x}(\sigma))}\right]$$

In this case, σ typically represents arc length along the characteristic or ray, and $\mathbf{x}(\sigma)$ is the position of the ray vector at the distance σ from the initial position of the ray. The process is usually initialized by setting $\mathbf{x}(0) = \mathbf{x}_s$ to the initial source position and setting, as shown in Equation 2-159.

(2-159) $$\mathbf{p}(0) = \frac{1}{v(\mathbf{x}_s)} \begin{pmatrix} \sin\alpha\cos\beta \\ \sin\alpha\sin\beta \\ \cos\alpha \end{pmatrix}$$

Once $\mathbf{x}(\sigma)$ is known, the desired traveltime is computed by integrating along the characteristic curve in Equation 2-160.

(2-160) $$\varphi(\mathbf{x}(\alpha,\beta,\sigma)) = \int_0^\sigma \frac{d\sigma'}{v^2(x(\alpha,\beta,\sigma'))}$$

Figure 2-35. Ray Fan versus Eikonal traveltime phase

(a). Ray Phase Function

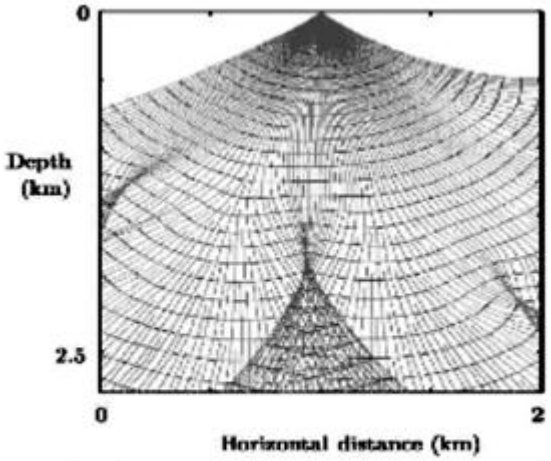

FIG. 8. A fan of rays in two dimensions starting from a surface location and the associated wavefronts. The ray coverage is kept sufficiently high by filling in shadows with new rays (see the section on wavefront construction).

(b). Eikonal Phase Function

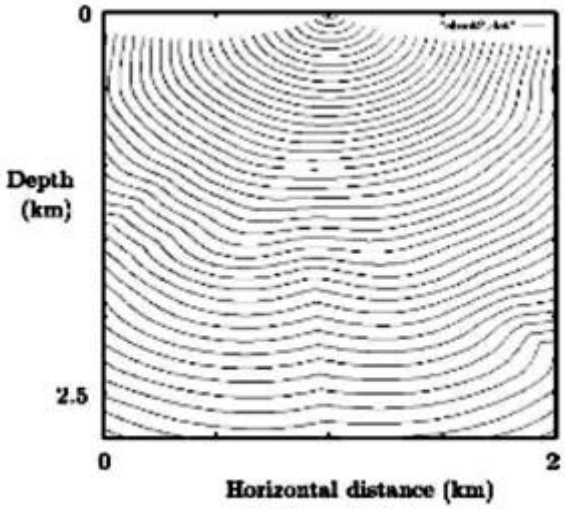

FIG. 10. Propagation of first-arrival wavefronts for the same shot and model as used in Figure 8.

Figure 2-36. Anisotropic model and traveltimes.

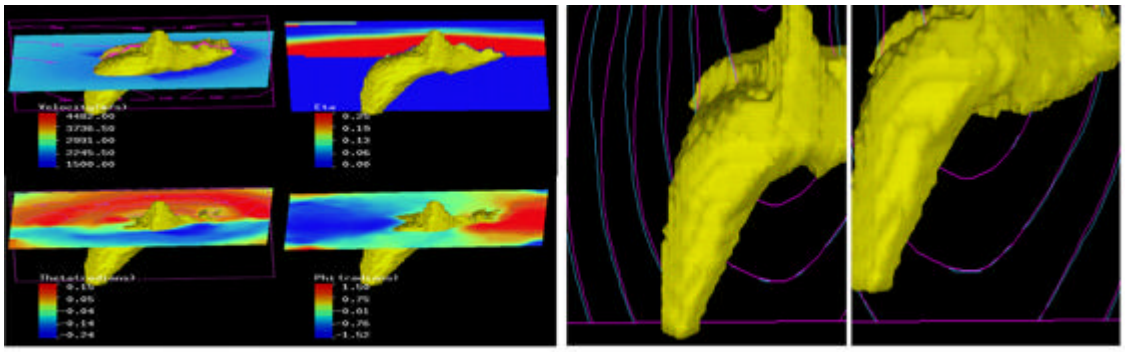

(a) Anisotropic Model

(b) Anisotropic Traveltimes

Raytrace Modeling

Figure 2-37(a) provides an example of how Huygens principle factors into construction of a raytrace-based response to exploding reflectors. Given a point on a reflecting surface (the red circle in the figure), a ray from a source point simulates an exploding the point. Rays emanate from the point in all directions and are recorded at surface receivers. Since any reflecting surface can be considered as a set of such points, the sum of all their point responses will produce, in the worst case, a reasonable approximation of what we would see if we ran our full two-way propagator for this model.

Figure 2-37. Huygens Principle as it applies to raytrace modeling

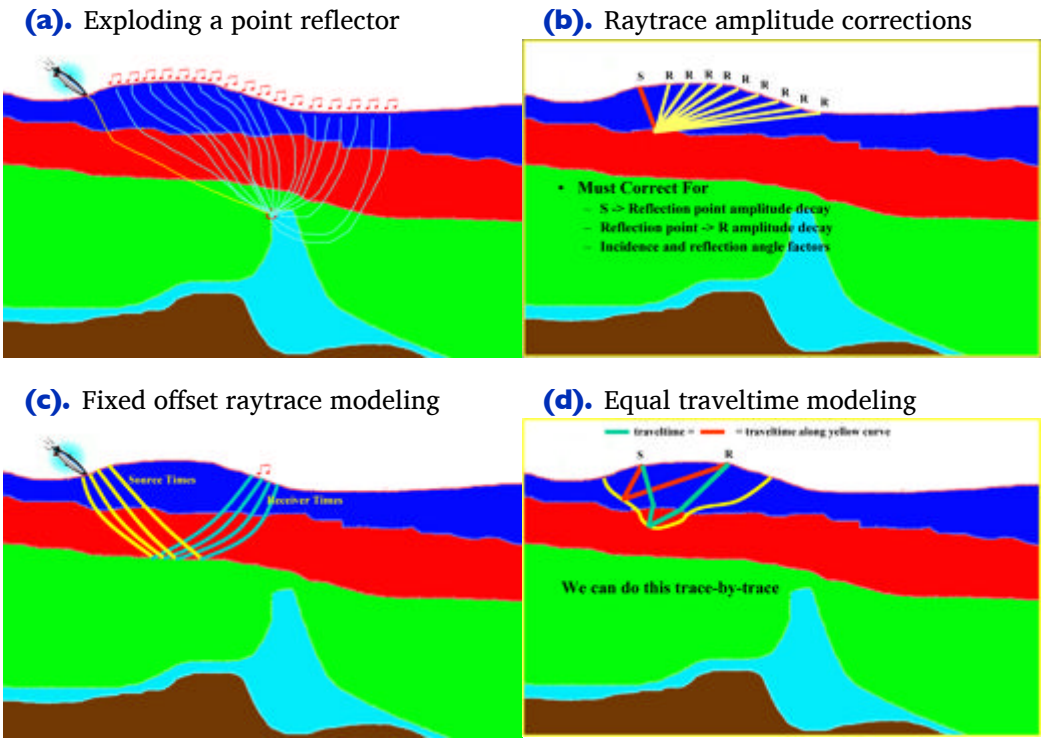

Figure 2-37(b) hints at one of the more complicated parts of accurate raytrace modeling. Reasonably accurate raytrace amplitude responses require that we correct for several important factors. These include source-to-reflection point decay and reflection-point-to-receiver amplitude decay, as well as obliquity factors based on the incidence and reflection angles. The phase of secondary arrivals also require correction.

Depending on how it is structured, raytrace modeling can be one of the most computationally efficient modeling methods available, and can easily model virtually any type of recording geometry. As indicated in Figure 2-37(c), raytrace modeling is easily modified to achieve fixed or common offset modeling. Its chief drawback is that multiples and other multiple arrival events are very difficult to include in the model.

While we tend to think of raytrace modeling in the sense of the isochron in Figure 2-37(a), this may not be optimum. Figure 2-37(d) shows raytrace modeling formulated in terms of equal traveltime curves or surfaces. The yellow curve in this figure represents all the reflection points for which the sum of the traveltime from a source to any point on the yellow line and back to a receiver is identical to that from any other reflection point. To produce the amplitude response at this time requires only that we sum all reflection amplitudes at these locations into the trace at this fixed time. If you already understand Kirchhoff migration to some degree, this concept should be very familiar.

Figure 2-38 provides proof of concept that the ray-based synthesis methods outlined here actually work. In this figure, the model is on the left and the ray based synthetic shot is on the right. The phase function, φ, and amplitude decays, A, were calculated using the method of characteristics along with a simultaneous solution to the transport equation.

Figure 2-38. A raytrace shot over the SEG AA′ 2D model.

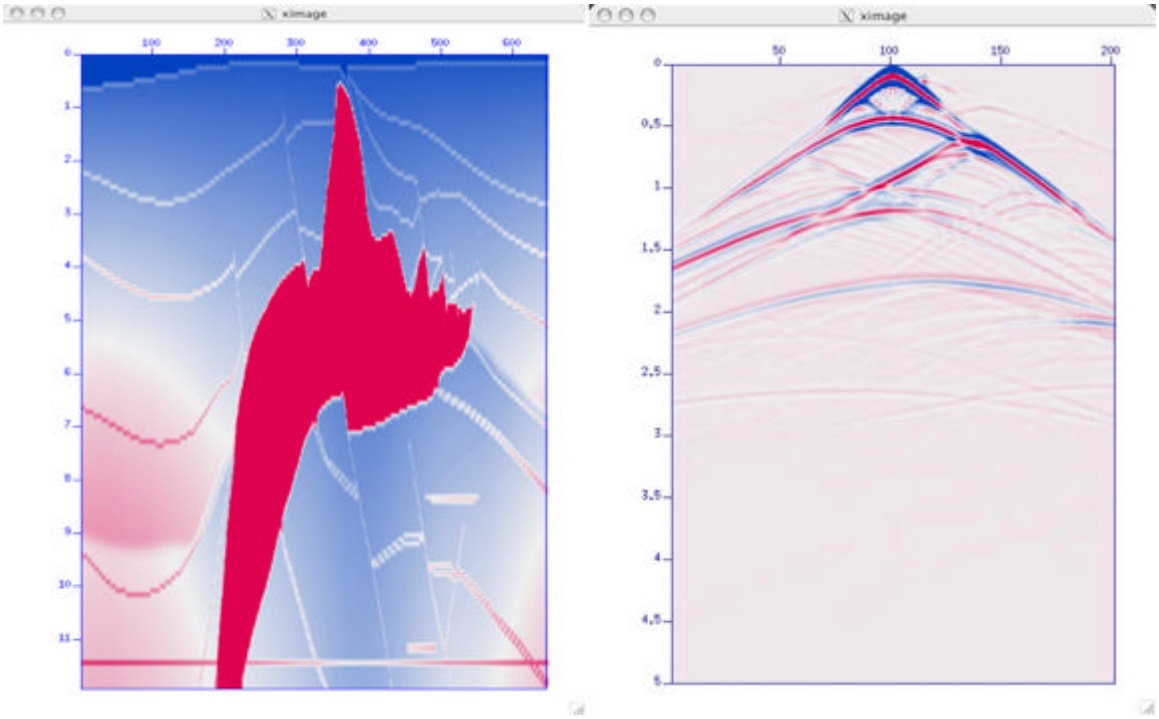

While the raypath concept is sufficient to understand plane wave issues, in most cases, we emphasize that the full plane wave generated by the source is much more complicated. Because of this fact, it is possible to generate a full wave response from an appropriately sampled bundle of ray theoretic plane waves. Figure 2-39 demonstrates this in terms of what are more precisely called *Gaussian beams*. What we see in this figure is part of the full response due to two plane wave raypaths. The blue lines indicate what are called central rays, while the red lines indicate wavefronts calculated directly from the central rays. The wavefronts are actually calculated using a finite difference technique specified by theoretical formulas analogous to those on which our one and two-way propagators are based. In addition to dynamically determining the amplitude

at each point on the red lines, a Gaussian weight is applied to ensure that the sum of all such waves faithfully represents the forward traveling wavefront. The name Gaussian beam is derived from this weighting methodology.

Figure 2-39. A partial wave response due to two rays.

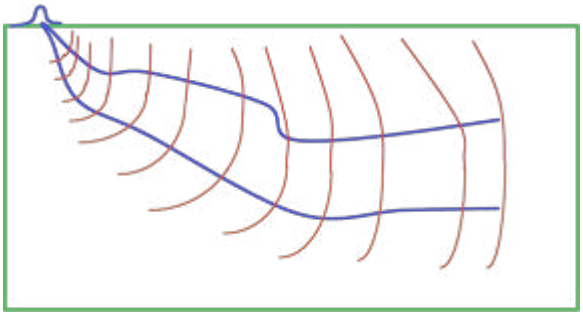

Figure 2-40 shows the kinds of events that each of our schemes can model successfully.

Figure 2-40. A brief comparison of modeling methods.

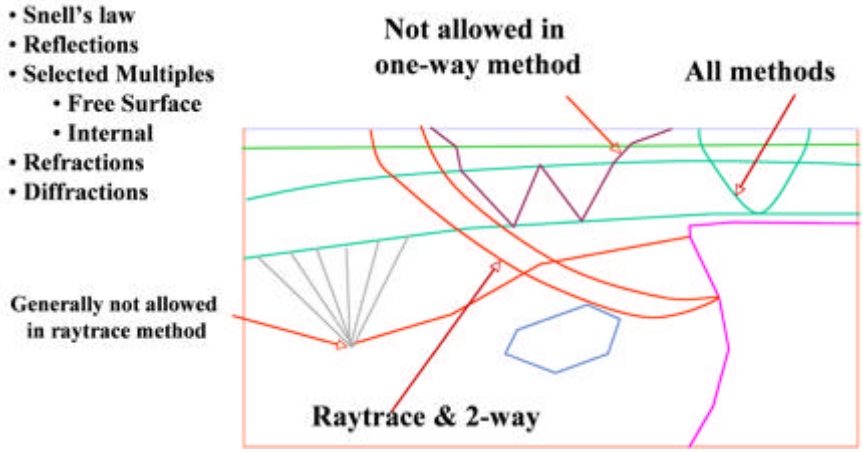

Figure 2-41 summarizes the differences between three modeling algorithms. The left hand side represents full two-way propagation, the middle image shows one-way propagation, and the right side shows single arrival raytrace-based modeling. Note that neither the full one-way nor the single arrival raytrace-based response have any reflected waves.

Figure 2-41. Basic model differences. Left is full two-way, middle is one-way, and right is single arrival Kirchhoff shot response for shot in center of model.

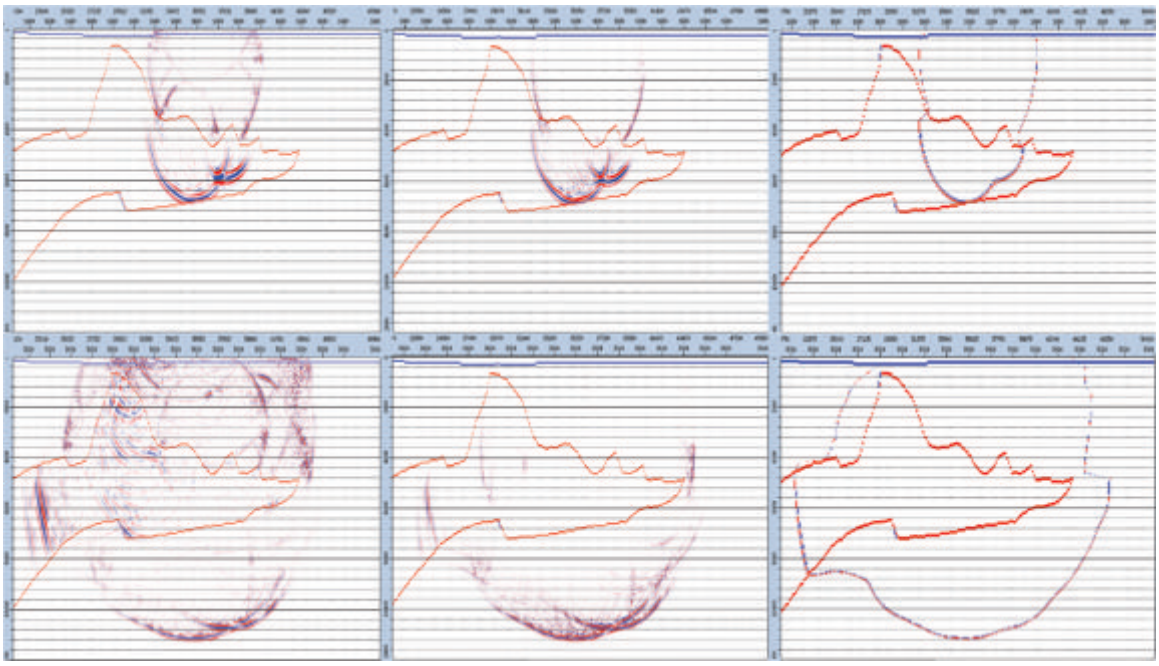

Zero Offset Modeling

At this point, our understanding of modeling is based on a two-step process. A source of some kind is initiated at time, $t = 0$, and it is then allowed to propagate into the Earth according to some form of propagating equation. We also understand that each subsurface point in the Earth, whether part of a reflector or not, can be considered as a point reflector. After some length of time, energy from the source reaches the point, and, according to Huygens Principle, initiates a new source at the location of the point reflector. The point reflector then acts as a internal source which radiates energy in all directions. Some of this energy reaches the surface as a reflection and some of it continues into the Earth to ignite other point reflectors creating additional sources until the energy is exhausted. What we record at the surface is the reflected energy at a widespread array of receivers with some offset from the source position. What we lose is the energy that never manages to get reflected. In such synthetic experiments, we can record all the information we want. If desired, we can even record zero-offset data, but to do that we have to set off sources at each location where we want a receiver. This means that, at considerable computational expense, we must forward propagate a source for every coincident receiver location.

In the early days of reflection seismic processing and interpretation, there was seldom enough computer power to produce an appropriate number of shots to enable synthesis of stacked sections. It was natural to attempt to find a way to produce all the traces in zero or short offset ensembles. It does not take much effort to come up with a reasonable approach. The Huygens principle tells us that if we can determine the response from any single subsurface point, all we have to do to produce the receiver wavefield is to sum all such responses into the receiver and we are done.

Let's consider the zero-offset response of a single point-reflector. If the traveltime from the source at s_i to the point-reflector at r is $t_{s_i r}$, the traveltime from the reflector back to the source is also $t_{s_i r}$ because the energy reaching the receiver at the source position must travel the path (or paths) from the source to the point-reflector in reverse. This means that the total traveltime from the source to the reflecting point and back to the receiver at the coincident source location is just $2t_{s_i}$. This statement must be true for every coincident source and receiver on the recording surface, so the zero offset response of the point reflector is the sum of the response for each source, s_i, on the recording surface.

The trick to understanding how to efficiently synthesize zero-offset responses is simply to realize that if the velocity, v, of the medium is divided by two and we set off an explosion at the point reflector at $t = 0$, then what we will record on the recording surface is exactly the time $2t_{s_i}$. Thus, exploiting Huygens Principle in Figure 2-33, the zero offset response for any given model can be obtained by simply dividing the velocity by two, setting off explosions at each subsurface point reflector, and recording the response at the surface. The only problem with this trick is that the zero-offset response obtained in this fashion will have odd period multiples whenever a free-surface is present.

Figure 2-42 shows what happens in the subsurface, and Figure 2-43 shows what we get at the surface when we synthesize exploding-reflector-zero-offset data. The far upper left image shows the subsurface exploding reflectors just before they explode. The remaining figures demonstrate how the wavefield propagates to the receivers.

Figure 2-42. Exploding reflector synthesis.

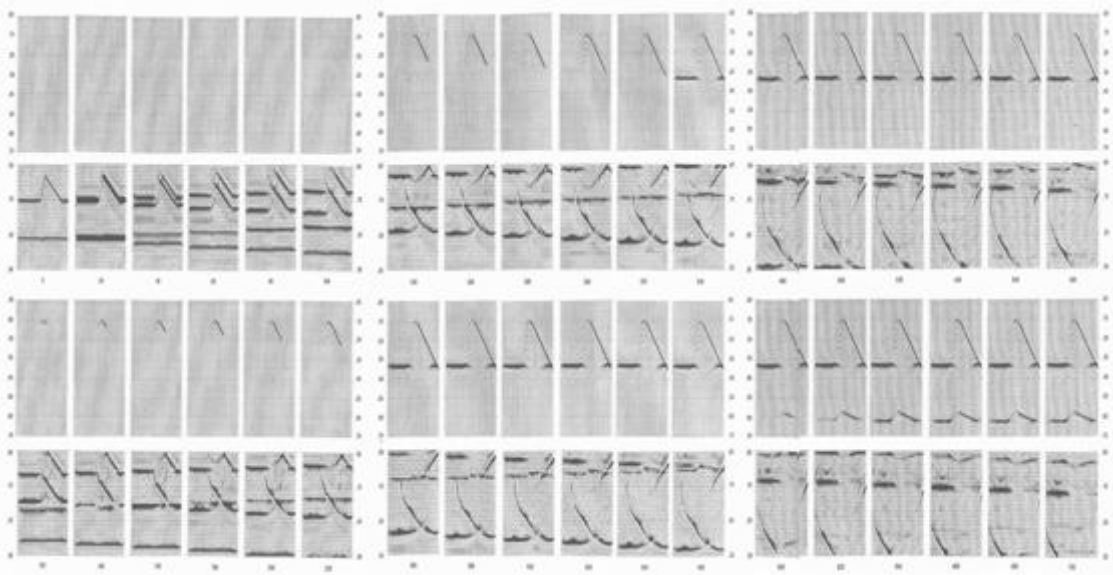

Figure 2-43. Surface response of the exploding reflectors from Figure 2-42

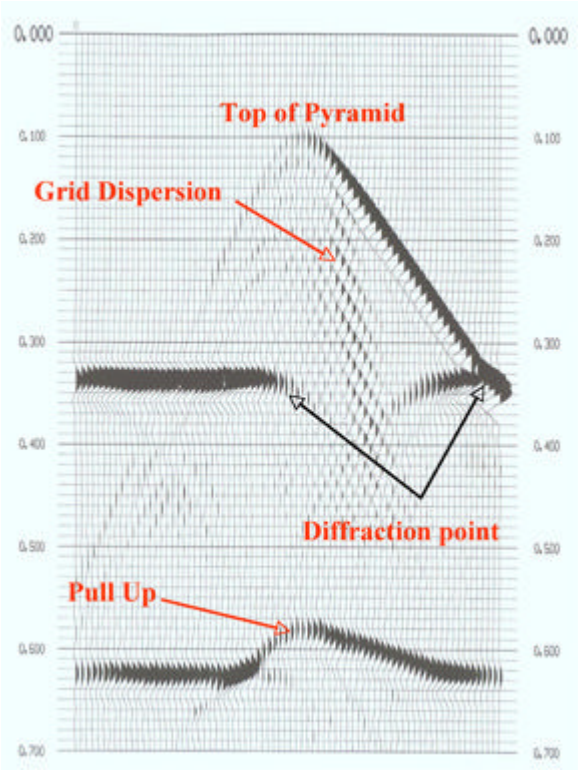

An easy way to understand the comments in the previous paragraph is through watching the movie schematized in Figure 2-44. This move was made in the late 1980's or early 1990's from a model derived from a 3D two-way migration of *DMO*-corrected Gulf of Mexico stacked data. It is based on what turned out to be an inaccurate interpretation of the salt flank, but it is still an interesting case study.

Figure 2-44. Exploding reflector movie. The best way to understand exploding reflector modeling is through a movie.